UC Davis

UC Davis Previously Published Works

Title

Atoh7-independent specification of retinal ganglion cell identity

Permalink

https://escholarship.org/uc/item/3hf7b5wz

Journal

Science Advances, 7(11)

ISSN

2375-2548

Authors

Brodie-Kommit, Justin
Clark, Brian S
Shi, Qing
et al.

Publication Date

2021-03-12

DOI

10.1126/sciadv.abe4983

Peer reviewed

eScholarship.org Powered by the California Digital Library
University of California

NEUROSCIENCE

Atoh7-independent specification of retinal ganglion cell identity

Justin Brodie-Kommit[1]*, Brian S. Clark[2,3]*, Qing Shi[4†], Fion Shiau[2], Dong Won Kim[5], Jennifer Langel[6], Catherine Sheely[1], Philip A Ruzycki[2], Michel Fries[7,8], Awais Javed[7,8], Michel Cayouette[7,8,9,10], Tiffany Schmidt[11], Tudor Badea[12,13], Tom Glaser[14], Haiqing Zhao[1], Joshua Singer[4], Seth Blackshaw[5,15,16,17‡], Samer Hattar[6‡]

Copyright © 2021 The Authors, some rights reserved; exclusive licensee American Association for the Advancement of Science. No claim to original U.S. Government Works. Distributed under a Creative Commons Attribution NonCommercial License 4.0 (CC BY-NC).

Retinal ganglion cells (RGCs) relay visual information from the eye to the brain. RGCs are the first cell type generated during retinal neurogenesis. Loss of function of the transcription factor *Atoh7*, expressed in multipotent early neurogenic retinal progenitors leads to a selective and essentially complete loss of RGCs. Therefore, *Atoh7* is considered essential for conferring competence on progenitors to generate RGCs. Despite the importance of Atoh7 in RGC specification, we find that inhibiting apoptosis in *Atoh7*-deficient mice by loss of function of *Bax* only modestly reduces RGC numbers. Single-cell RNA sequencing of *Atoh7;Bax*-deficient retinas shows that RGC differentiation is delayed but that the gene expression profile of RGC precursors is grossly normal. *Atoh7;Bax*-deficient RGCs eventually mature, fire action potentials, and incorporate into retinal circuitry but exhibit severe axonal guidance defects. This study reveals an essential role for *Atoh7* in RGC survival and demonstrates *Atoh7*-dependent and *Atoh7*-independent mechanisms for RGC specification.

INTRODUCTION

The retina has six major classes of neurons that develop from a common progenitor cell pool during overlapping temporal intervals. Retinal ganglion cells (RGCs), the only projection neurons from the retina to the brain, are the first retinal cell type to be generated. RGC development in zebrafish, mice, and humans has been shown to require the basic helix-loop-helix transcription factor atonal homolog 7, *Atoh7* (*Math5*) (*1*–*8*). *Atoh7* is conserved across all vertebrate species and distantly related to *atonal*, which specifies the earliest-born neurons in *Drosophila* retina (*1*, *3*, *7*, *9*). *Atoh7*-deficient mice and zebrafish lack upward of 95% of RGCs (*1*, *8*, *10*, *11*) and likewise lack any visible optic nerve or functional connections from the retina to the brain (*12*, *13*). Human mutations in *ATOH7* or its cis-regulatory regions have been associated with optic nerve agenesis or hypoplasia (*4*, *6*, *14*) and increased susceptibility to glaucoma (*15*, *16*). *Atoh7* deficiency also disrupts the development of retinal vasculature in both mice and humans, likely as an indirect result of the loss of RGCs (*17*, *18*).

In mice, *Atoh7* is expressed in neurogenic retinal progenitor cells (RPCs) between E12 and P0, corresponding to the interval in which RGCs are generated (*8*, *19*–*26*). Upon cell fate specification, *Atoh7* expression is rapidly down-regulated in mouse RGC precursors (*23*, *27*) although expression persists in immature human RGCs (*28*, *29*). Genetic fate mapping indicates that *Atoh7*-expressing RPCs also give rise to other early-born retinal cells, including cone photoreceptors, horizontal, and amacrine cells, and that generation of these cell types is increased in *Atoh7*-deficient mice (*1*, *8*, *12*, *30*). Although it has been reported that ectopic expression of *Atoh7* can promote RGC formation in some situations (*22*, *31*), it is typically not sufficient to drive RGC specification (*22*, *30*, *32*–*38*). However, misexpression of *Atoh7* in *Crx*-expressing photoreceptor precursors was sufficient to rescue the development of a limited number of RGCs (*22*).

These findings have suggested that *Atoh7* acts in neurogenic RPCs to confer competence to generate RGCs (*10*, *39*, *40*) potentially in combination with as yet unidentified factors. Recent experiments have shown that when *Pou4f2* and *Isl1* are expressed under the control of the endogenous *Atoh7* promoter, these transcription factors are sufficient to fully rescue the defects in RGC development seen in *Atoh7* mutants (*32*, *34*, *37*). This implies that *Atoh7* may act permissively to enable the expression of these two factors in early-stage RPCs in order to generate RGCs.

Other data, however, suggest that a large number of RGCs are specified independently of *Atoh7*. Previous studies indicate that immature RGCs are present in *Atoh7*-deficient mice in embryonic retina, although at reduced numbers relative to controls (*1*, *10*). Genetic fate-mapping studies further raise questions about the necessity of *Atoh7* for specification of all RGC subtypes. Analysis of *Atoh7-Cre* knock-in mice reveals that only 55% of all RGCs are generated from *Atoh7*-expressing RPCs (*10*, *25*, *41*). Although this outcome may reflect inefficient activation of Cre-dependent reporter constructs, it may also imply that a subset of RGCs are specified through an *Atoh7*-independent mechanism. However, the loss of

[1]Department of Biology, Johns Hopkins University, Baltimore, MD, USA. [2]John F. Hardesty, MD, Department of Ophthalmology and Visual Sciences, Washington University School of Medicine, St. Louis, MO, USA. [3]Department of Developmental Biology, Washington University School of Medicine, St. Louis, MO, USA. [4]Department of Biology, University of Maryland, College Park, MD, USA. [5]Department of Neuroscience, Johns Hopkins University School of Medicine, Baltimore, MD, USA. [6]National Institute of Mental Health (NIMH), National Institutes of Health (NIH), Bethesda, MD, USA. [7]Cellular Neurobiology Research Unit, Institut de Recherches Cliniques de Montréal, Montréal, QC H2W 1R7, Canada. [8]Molecular Biology Programs, Université de Montréal, QC H3C 3J7, Canada. [9]Department of Anatomy and Cell Biology, McGill University, Montréal, QC H3A 0G4, Canada. [10]Department of Medicine, Université de Montréal, Montréal, QC H3T 1J4, Canada. [11]Department of Neurobiology, Northwestern University, Evanston, IL, USA. [12]National Eye Institute, National Institutes of Health, Bethesda, MD, USA. [13]Research and Development Institute, Transylvania University of Brasov, School of Medicine, Brasov, Romania. [14]Department of Cell Biology and Human Anatomy, University of California, Davis School of Medicine, Davis, CA, USA. [15]Department of Neurology, Johns Hopkins University School of Medicine, Baltimore, MD, USA. [16]Department of Ophthalmology, Johns Hopkins University School of Medicine, Baltimore, MD, USA. [17]Kavli Neuroscience Discovery Institute, Johns Hopkins University, Baltimore, MD, USA.
*These authors contributed equally to this work.
†Present address: Department of Chemical Physiology and Biochemistry, Oregon Health and Science University, Portland, OR, USA.
‡Corresponding author. Email: samer.hattar@nih.gov (S.H.); sblack@jhmi.edu (S.B.)

95% of RGCs in *Atoh7* mutant retinas may suggest that Atoh7-independent RGCs require trophic support from either *Atoh7*-expressing RPCs or *Atoh7*-derived RGCs.

To distinguish the role of *Atoh7* in controlling RGC specification and survival, we prevented RGC death in *Atoh7*-deficient mice by simultaneously inactivating the proapoptotic gene *Bax* (*42*, *43*). The idea being if RGCs can be specified in the absence of *Atoh7* but require it for trophic support, we should reveal RGCs that are specified in an Atoh7-independent manner when cell death is prevented. Notably, we observed only a 25.2 ± 0.9% reduction in adult RGC numbers in $Atoh7^{-/-}$;$Bax^{-/-}$ retinas relative to $Bax^{-/-}$ controls, implicating an unrecognized Atoh7-independent specification pathway for RGCs. While mutant RGCs showed severe defects in the formation of axonal projections and retinal vasculature, we found that the Atoh7-independent RGCs expressed both *Pou4f2* and *Isl1*, the two transcription factors that are sufficient to fully compensate for Atoh7 function. These RGCs also fired action potentials in response to light and formed functional synapses with upstream retinal neurons. Single-cell RNA sequencing (scRNA-Seq) analysis of *Atoh7;Bax*-deficient retinas shows that *Atoh7*-deficient RGC differentiation is delayed relative to wild type (WT), implicating Atoh7 as responsible for generating early-born pioneering RGCs. Last, Cut&Run analysis indicates that Atoh7 directly activates genes enriched in RGC precursors while directly repressing genes enriched in neurogenic RPCs and photoreceptor precursors. Our results both identify a pathway for specifying RGCs that is independent of Atoh7 and clarify the mechanism of Atoh7 function during early retinal neurogenesis.

RESULTS

Atoh7 promotes RGC survival, but RGC specification is largely *Atoh7* independent

In the absence of *Atoh7*, there is an increase in apoptosis of both *Atoh7*-derived cells across embryonic retinal development and non–*Atoh7*-derived cells in the ganglion cell layer (GCL) at embryonic day 16.5 (E16.5) and E17.5 (*22*, *25*). These data suggest that Atoh7 may promote RGC survival in both a cell-autonomous and a non–cell-autonomous manner. To better understand the role that Atoh7 plays in RGC development, independent of its role in RGC survival, we disrupted both *Atoh7* and the proapoptotic *Bax* gene in order to inhibit apoptosis in the retina.

We used $Atoh7^{Cre/Cre}$ mice, in which the *Atoh7* coding sequence is replaced with Cre recombinase via targeted recombination, generating a null allele, to analyze Atoh7 function (*40*). We first examined the expression of RBPMS and Isl1, both of which are broadly expressed in RGCs, in $Atoh7^{Cre/Cre}$;$Bax^{-/-}$ mice (hereafter referred to as $Atoh7^{-/-}$;$Bax^{-/-}$ mice) (Fig. 1, A to C). *Isl1*, a LIM family homeodomain transcription factor, is necessary for RGC development and maintenance in adulthood (*32*, *44*) and is expressed in mature RGCs, bipolar, and amacrine cells. Using anti-Rbpms to selectively label all RGCs, we observed a 159 ± 7% (Fig. 1, A and B) increase in RGC number in $Bax^{-/-}$ retinas, in line with previous results indicating that RGCs undergo extensive levels of apoptosis during development (*45*–*47*). However, we observe only a 25.2 ± 0.9% reduction in RGCs in $Atoh7^{-/-}$;$Bax^{-/-}$ relative to $Bax^{-/-}$ retinas. This contrasts with the 99.54 ± 0.12% reduction in RGCs in $Atoh7^{-/-}$ retinas compared to controls (Fig. 1, A and B). Similar results were observed for anti-Isl1 cells in the GCL (Fig. 1, A and C).

Specific RGC markers, Brn3a (Pou4f1) and Brn3b (Pou4f2), were used to quantify RGCs. For WT and $Bax^{-/-}$ lines, Brn3a and Brn3b numbers were similar to published reports (Fig. 1, D to F) (*8*, *22*, *48*, *49*). In the $Atoh7^{-/-}$ line, a 99.8 ± 0.2% reduction in Brn3a RGC density was observed. However, in $Atoh7^{-/-}$;$Bax^{-/-}$ mice, the Brn3a RGCs were substantially rescued in the $Atoh7^{-/-}$ background and remained into adulthood. Brn3a RGCs (74.7 ± 0.9%) are rescued in $Atoh7^{-/-}$;$Bax^{-/-}$ mice relative to $Bax^{-/-}$ levels in adult, and RGCs display normal distribution across the entire retina (Fig. 1, D and E; fig. S1, A and A′; and fig. S2). Brn3b RGCs were also rescued in $Atoh7^{-/-}$;$Bax^{-/-}$ relative to $Bax^{-/-}$ retinas, but to a much lesser extent than the Brn3a (28.8 ± 5.9%; Fig. 1, D and F, and fig. S1, B and B′). Expression of *Isl1*, *Brn3b*, and, to a lesser extent, *Brn3a* has previously been reported to require *Atoh7* (*32*, *37*, *39*, *44*, *48*, *50*). However, our data demonstrate that the expression of *Isl1*, *Brn3a,* and *Brn3b* in RGCs can occur independent of *Atoh7* (Fig. 1).

To investigate the extent to which rescued RGCs resembled WT neurons, we examined the expression of markers of major classes of mature RGCs. We investigated the prevalence of intrinsically photosensitive RGCs (ipRGCs) within $Atoh7^{-/-}$;$Bax^{-/-}$ retinas. During the development of ipRGCs, most cells express Brn3b, although, in some cases, only transiently (*51*). To determine the percentage of rescued ipRGCs in $Atoh7^{-/-}$;$Bax^{-/-}$ mice, we used a melanopsin antibody that predominantly labels the high melanopsin-expressing M1 and M2 ipRGC populations. We observe that 34.1% of ipRGCs are rescued in $Atoh7^{-/-}$;$Bax^{-/-}$ mice relative to $Bax^{-/-}$, proportions similar to the fraction of Brn3b-positive RGCs in WT (Fig. 1, D and F, and fig. S1, C to F). This indicates that rescued Brn3b-positive ipRGCs can differentiate in the absence of *Atoh7*.

To eliminate the possibility that global loss of function of *Bax* caused a nonspecific rescue of RGC development, we tested the effects of retina-specific conditional mutants of *Bax*, using *Chx10-Cre;* $Atoh7^{Cre/Cre}$;$Bax^{fl/fl}$ (Fig. 1, G and H). In this model, *Bax* is selectively disrupted in RPCs beginning at E10 to 10.5 (*52*). Removal of *Bax* from all RPCs shows RGC development to the same extent as in $Atoh7^{Cre/Cre}$;$Bax^{-/-}$ (Fig. 1, G and H). This indicates that the rescue of RGCs is specific to the retina.

We then reasoned that if cell death has to be rescued specifically in Atoh7-independent RGCs, then the number of RGCs should not be restored in $Atoh7^{Cre/Cre}$;$Bax^{fl/fl}$ mice. We observed that $Atoh7^{Cre/Cre}$; $Bax^{fl/fl}$ mice did not show any notable rescue of RGC numbers (Fig. 1, G and H), suggesting that preventing cell death in cells that do not express *Atoh7* is sufficient for RGCs to differentiate and form connections with retinal neurons.

In both WT and $Atoh7^{-/-}$;$Bax^{-/-}$ animals, we observe that 34 ± 11% and 34 ± 26% of RGCs, respectively, are derived from Atoh7-expressing cells, a finding that independently confirms similar lineage tracings in previous studies (fig. S3, A to C) (*10*, *25*). This indicates that while RGCs that are normally derived from *Atoh7*-expressing neurogenic RPCs are reduced in the absence of *Atoh7*, *Atoh7* is not required for their specification. Furthermore, RGCs that are derived from non–*Atoh7*-expressing RPCs require *Atoh7* for survival through a non–cell-autonomous mechanism.

While RGCs were the main focus of this study, Atoh7-expressing progenitors also give rise to other early-born retinal cell types (*1*, *12*), so we investigated whether these cell types were affected in the adult $Atoh7^{-/-}$;$Bax^{-/-}$ retina. Using immunostaining for cell type–specific markers, we observed no notable difference between cone photoreceptors across any genotype (fig. S4, A and B). We observed a

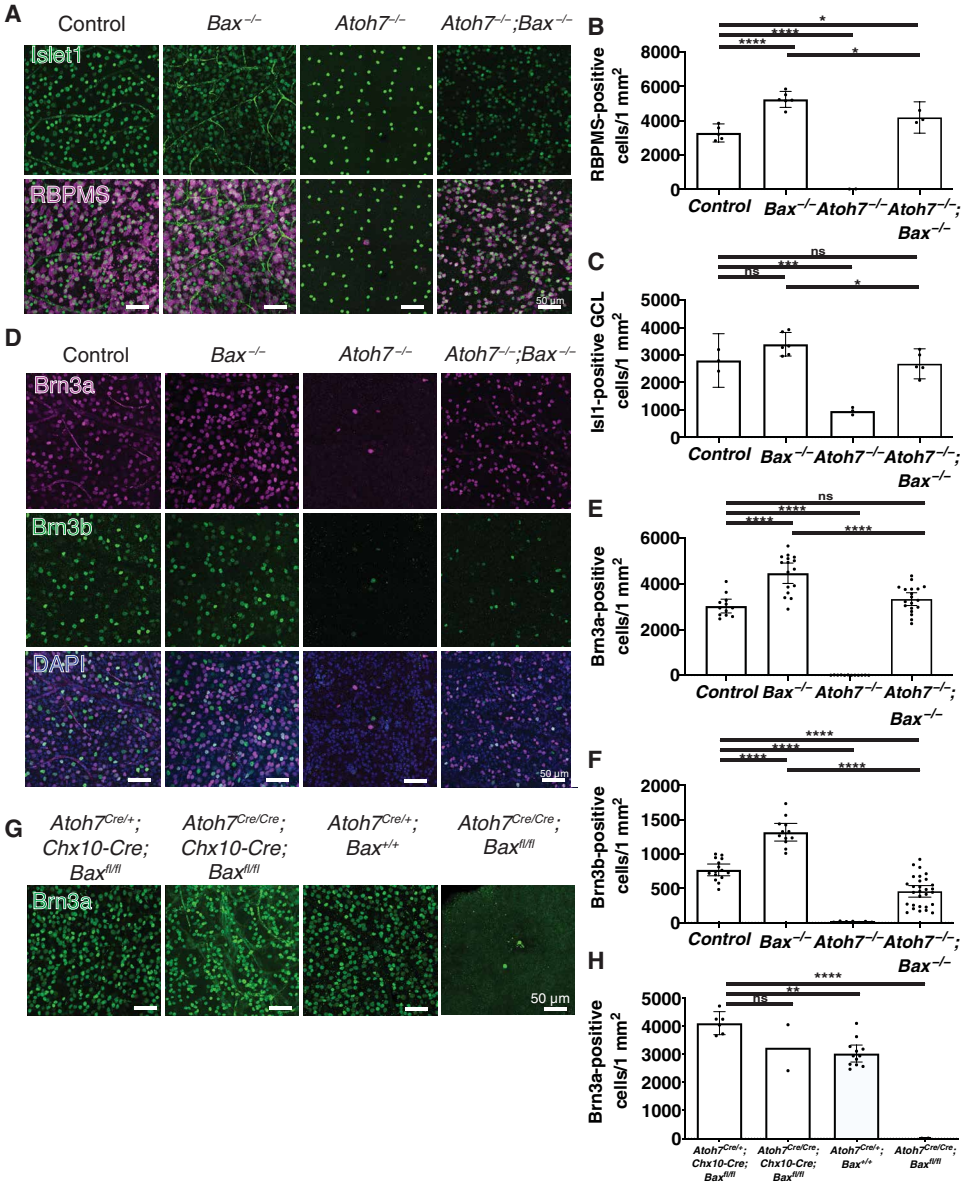

Fig. 1. Atoh7-independent development of RGCs. (**A** to **C**) We observed a 25.2 ± 0.9 and 21 ± 3% reduction in RBPMS$^+$ RGC density or Isl1$^+$ GCL cells when comparing *Atoh7*$^{-/-}$;*Bax*$^{-/-}$ to *Bax*$^{-/-}$ mice. (**D** to **H**) Brn3a- and Brn3b-positive RGC density are only moderately reduced when apoptosis is blocked in *Atoh7*$^{-/-}$;*Bax*$^{-/-}$ mice. (G and H) Brn3a-positive RGC numbers are rescued when apoptosis is blocked in all neural RPCs, when *Bax*$^{lox/lox}$ is crossed to the *Chx10-Cre* transgene, which is expressed in all RPCs. However, when *Bax* is specifically removed in *Atoh7-Cre* knock-in mice, Brn3a RGCs are not rescued. Means ± 95% confidence intervals. Statistical significance tested by one-way analysis of variance (ANOVA) with Tukey's posttest for multiple comparisons **P* < 0.045, ***P* = 0.0023, ****P* < 0.0003, *****P* < 0.0001. ns, non-significant.

significant decrease in horizontal cells in the *Atoh7*$^{-/-}$;*Bax*$^{-/-}$ compared with *Atoh7*$^{-/-}$ but neither with control nor with *Bax*$^{-/-}$ (fig. S4, C and E). We observed a notable decrease in amacrine cells in the *Atoh7*$^{-/-}$;*Bax*$^{-/-}$ retinas compared with both control and *Bax*$^{-/-}$ mice, although no notable differences were observed between control and *Atoh7*$^{-/-}$ (fig. S4, C and E). These results stand in contrast to a previous study that reported an increase in cone photoreceptors in adult *Atoh7*$^{-/-}$ retinas (*1*) and may reflect technical differences resulting from the use of different cone-specific markers (S-opsin) and quantification of dissociated cells, rather than cones in intact retina. In any case, these data clearly demonstrate that RGCs are the only early-born retinal cell type whose levels are substantially increased by the loss of function of *Atoh7* in the *Bax* mutant background.

RGCs specified in the absence of *Atoh7* generate light-driven photic responses transduced from the outer retina

As we determined that loss of Bax in the *Atoh7*$^{-/-}$ background rescues a large percentage of RGC specification, we next sought to investigate the degree to which RGCs differentiated in the absence of *Atoh7*. One hallmark of RGC differentiation is the formation of presynaptic contacts and the generation of light-induced action potentials. We used multielectrode array (MEA) recordings to test the light responsiveness of the RGCs within the various mutant

models. Spatiotemporal noise stimuli were used to activate the retina with a mean excitation of 398 nm ($I_{mean} \approx 5 \times 10^3$ photons cm^{-2} s^{-1}), a wavelength that predominantly activates S-cones (*53*) and does not activate *Opn4*-expressing ipRGCs (*54*–*57*). We observed an identical stimulus-response profile in WT and $Bax^{-/-}$ RGCs (Fig. 2A), an expected result given that $Bax^{-/-}$ mice display normal visual responses within the Morris water maze test (*42*). The population of RGCs included cells with similar light-evoked responses to ON sustained, ON transient, ON/OFF transient, OFF transient, or OFF sustained RGCs (Fig. 2A and fig. S5). The spatial receptive fields of the $Atoh7^{-/-};Bax^{-/-}$ RGCs were slightly smaller than normal [$Atoh7^{-/-};Bax^{-/-}$ average, 191 ± 37.1 μm (n = 56 from eight mice); control average, 212 ± 42.3 μm (n = 92 from five mice); and $Bax^{-/-}$ average, 223 ± 42.4 μm (n = 96 from four mice)] (Fig. 2B), and the kinetics of the light-driven responses in the $Atoh7^{-/-};Bax^{-/-}$ retinas were slightly slower than those of control and $Bax^{-/-}$cells (Fig. 2C).

The linear analysis used for the MEA data can only reveal an averaged spike-triggered averaging (STA), which could be a compression of multiple receptive fields. Thus, those having multiple receptive fields such as ON-OFF cells could potentially be hidden with this method and require more sophisticated analysis strategy (*58*). However, diversity in peristimulus time histogram (PSTH) profiles is clearly observed, suggesting that different cell types coexist in $Atoh7^{-/-};Bax^{-/-}$ mice. We chose not to perform more complex analysis such as classifying each cell into known cell types due to the relatively small sample size. These will be intriguing questions to address when larger amounts of data are made accessible. The near-normal properties of the $Atoh7^{-/-};Bax^{-/-}$ RGCs show that RGCs present in the $Atoh7^{-/-};Bax^{-/-}$ are wired properly to the outer retina, specifically the S-cones, and receive normal circuit input.

RGC axon guidance is *Atoh7* dependent

While RGCs in $Atoh7^{-/-};Bax^{-/-}$ animals appropriately respond to the detection of visual stimuli by the outer retina, the ability of these RGCs to form postsynaptic connections in the brain is compromised. We observed a substantially reduced pupillary light response (PLR) in $Atoh7^{-/-};Bax^{-/-}$ animals compared to controls (Fig. 3, B and C). To determine the cause of behavioral deficits, we assessed the distribution of RGC axons. Immunostaining for Smi32 (nonphosphorylated Nfh) (Fig. 3, A and D, and fig. S6C), Nfh, and Nfm (fig. S6, A and B) was used to evaluate RGC axonal integrity and showed normal architecture in WT and $Bax^{-/-}$ mice. We were surprised to find that the <1% of RGCs that survive in the $Atoh7^{-/-}$ showed severe guidance defects. These RGCs fasciculate, come in close proximity to where the optic disc should be, seem to overshoot the optic disc, and then continue to extend within the retina. The great majority of $Atoh7^{-/-}$ RGC axons fail to correctly target the optic disc, with only a few axons exiting and forming a rudimentary optic nerve, leading to a severely reduced PLR (Fig. 3, B and C, and fig. S7, A to C). The gross misguidance of axons was also observed in $Atoh7^{-/-};Bax^{-/-}$ mice (Fig. 3, A and D). As in $Atoh7^{-/-}$ mice, RGC axons in $Atoh7^{-/-};Bax^{-/-}$ mice fasciculate, fail to correctly target the optic disk, and form tracts that extend around the retina, with only rudimentary optic nerves observed. This guidance defect did not obviously result from the defective formation of the optic disc, as Pax2-positive glial cells that mark this structure are present in the $Atoh7^{-/-};Bax^{-/-}$ at E12.5 (fig. S8, A and B), although it is possible that other features of optic disc cells are disturbed. This demonstrates that the optic disk is present, but the axons are unable to find their way out of the retina in large numbers. These findings are reminiscent of previous reports in zebrafish, in which morpholino-mediated disruption of *atoh7* expression in early-stage RPCs disrupted the correct targeting of axons of later-born, *atoh7*-positive RGCs to the optic tectum (*33*).

Previous studies have observed a lack or massive reduction in physical or functional connection to the brain in $Atoh7^{-/-}$ mice (*1*, *12*, *13*, *59*). Consistent with the failure of mutant RGCs to correctly target the optic nerve, we observe severe disruptions in behavioral responses to light in $Atoh7^{-/-};Bax^{-/-}$ mice that are essentially indistinguishable from those seen in $Atoh7^{-/-}$ mice. $Atoh7^{-/-};Bax^{-/-}$ mice show no detectable optokinetic response (fig. S9A) and show no visual cue–dependent reduction in escape time during successive trials of the Morris water maze (fig. S9B). *Opn4:Tau-lacZ* knock-in mice, which visualize the axonal projections of M1 ipRGCs, show no detectable signal in the brain in $Atoh7^{-/-};Bax^{-/-}$ (fig. S9C) (*55*). Intraocular injection of fluorescently labeled cholera toxin beta, which visualizes RGC axonal terminals (*60*), likewise shows no brain labeling in both $Atoh7^{-/-};Bax^{-/-}$ and $Atoh7^{-/-}$ mice (fig. S9D). However, while the contralateral PLR is significantly reduced compared to WT in both the $Atoh7^{-/-}$ and $Atoh7^{-/-};Bax^{-/-}$ mice, it is, nonetheless, detectable, indicating that a small number of RGC axons target the olivary pretectal nucleus in $Atoh7^{-/-};Bax^{-/-}$ mice, although we are unable to detect these using standard techniques (Fig. 3, B and C, and fig. S7, A to C).

Retinal vasculature development is disrupted in the absence of *Atoh7*

In both mice and humans, loss of *Atoh7* expression results in persistence of the hyaloid vasculature (*2*, *7*, *17*, *61*). The persistence of the hyaloid vasculature in $Atoh7^{-/-}$ retinas until P14 was previously observed. We likewise observe persistence of the hyaloid vasculature into adulthood in $Atoh7^{-/-}$ retinas (Fig. 3E). Unexpectedly, even with the rescue of a majority of Brn3a RGCs in $Atoh7^{-/-};Bax^{-/-}$ animals, the hyaloid vasculature still fails to regress (Fig. 3E). Likewise, *Crx>Atoh7*;$Atoh7^{-/-}$ mice, in which *Atoh7* is misexpressed in photoreceptor precursors, also fail to induce hyaloid regression (Fig. 3E). This is in sharp contrast to the rescued vascular phenotype observed in $Atoh7^{tTA/tTA}$;*B&I-EE* mice, when *Brn3b* and *Isl1* are ectopically expressed from the endogenous *Atoh7* locus in a *Atoh7*-deficient mouse using the tet-off system (Figure 3E) (*37*), and implies that *Brn3b* and *Isl1* may activate the expression of secreted factors that drive vascular regression in a narrow time window during development.

scRNA-seq analysis of RGCs generated in the absence of *Atoh7*

To examine potential differences in RGC development within $Atoh7^{-/-}$ and $Atoh7^{-/-};Bax^{-/-}$ compared to WT and $Bax^{-/-}$ control animals, we next performed scRNA-seq on $Bax^{-/-}$, $Atoh7^{-/-}$, and $Atoh7^{-/-};Bax^{-/-}$ retinas to more comprehensively profile changes in cell-type specification and global transcriptome across the genotypes. We profiled 67,050 E14.5 retinal cells from $Bax^{-/-}$, $Atoh7^{-/-}$, and $Atoh7^{-/-};Bax^{-/-}$ mice and aggregated the datasets with 26,078 age-matched WT retinal cells from previous studies (Fig. 4, A and B, and fig. S10) (*23*). Consistent with the previous single-cell studies of E14 mouse retinal development (*23*, *62*), in low-dimension space, we observed a continuous manifold of cells, from primary RPCs to neurogenic RPCs, leading to three separate differentiation trajectories that give rise to RGCs, cones, and amacrine/horizontal cells, respectively

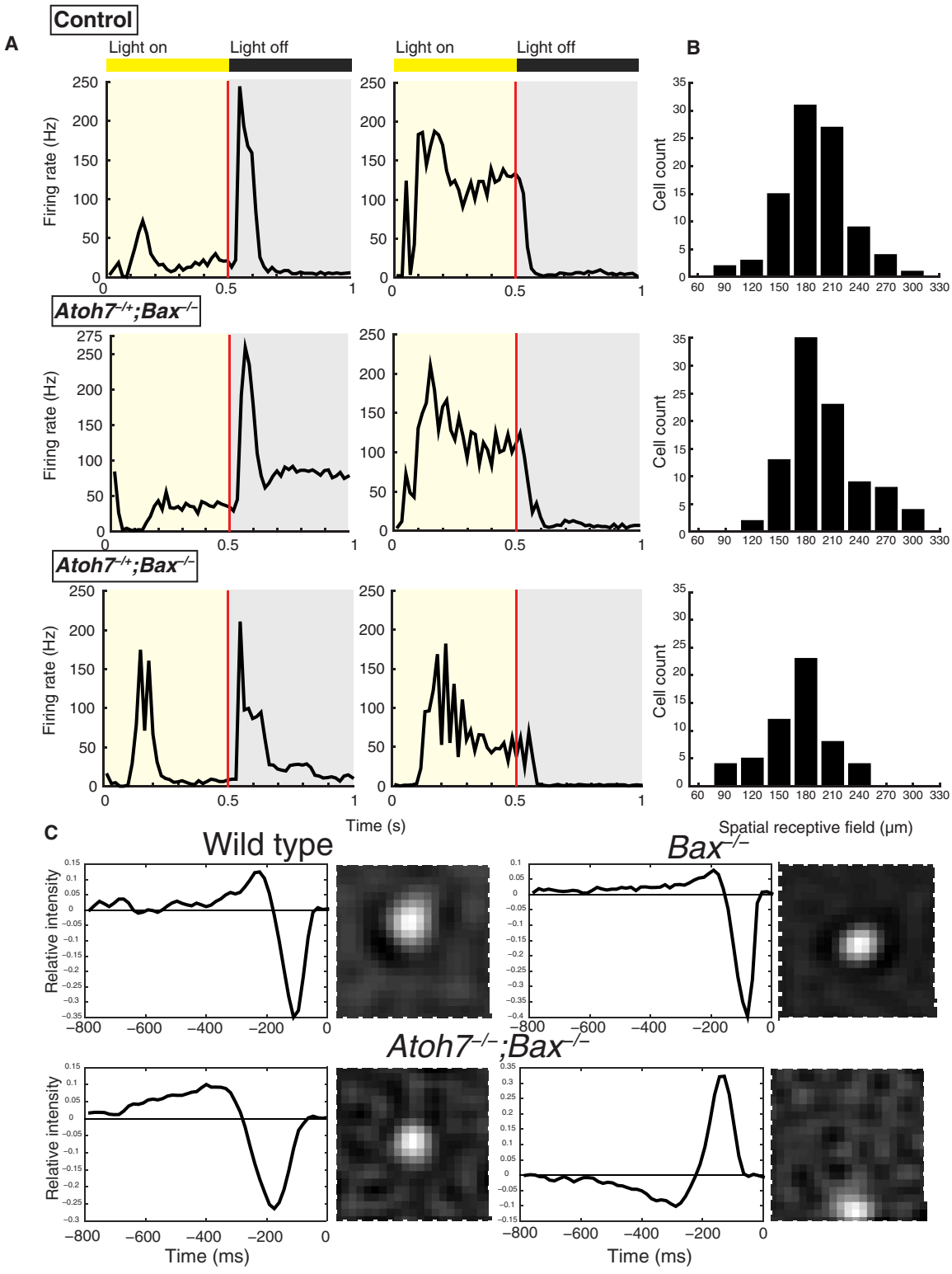

Fig. 2. *Atoh7* is not required for normal retinal wiring and electrophysiological function. Cells from *Atoh7*$^{+/-}$;*Bax*$^{-/-}$ and *Atoh7*$^{-/-}$;*Bax*$^{-/-}$ mice responded to light similarly to those from WT. (**A**) Two different examples, corresponding to two different sets of RGCs per genotype of peristimulus time histogram (PSTH) averaged from 120 repetitions of 1-Hz square-wave flash: WT (top), *Atoh7*$^{+/-}$;*Bax*$^{-/-}$ (middle), and Atoh7$^{-/-}$;Bax$^{-/-}$ (bottom). (**B**) Distribution of the spatial receptive field measured using white noise flickering checkerboard: WT (top; cell count = 92), *Atoh7*$^{+/-}$;*Bax*$^{-/-}$ (middle; cell count = 94), and *Atoh7*$^{-/-}$;*Bax*$^{-/-}$ (bottom; cell count = 56). (**C**) The PSTH of responses to square-wave flash was calculated using 10-ms bins. Mice were assayed at P30. One-way ANOVA, followed by Dunnett's test, $P < 0.05$, between *Atoh7*$^{-/-}$;*Bax*$^{-/-}$ and WT.

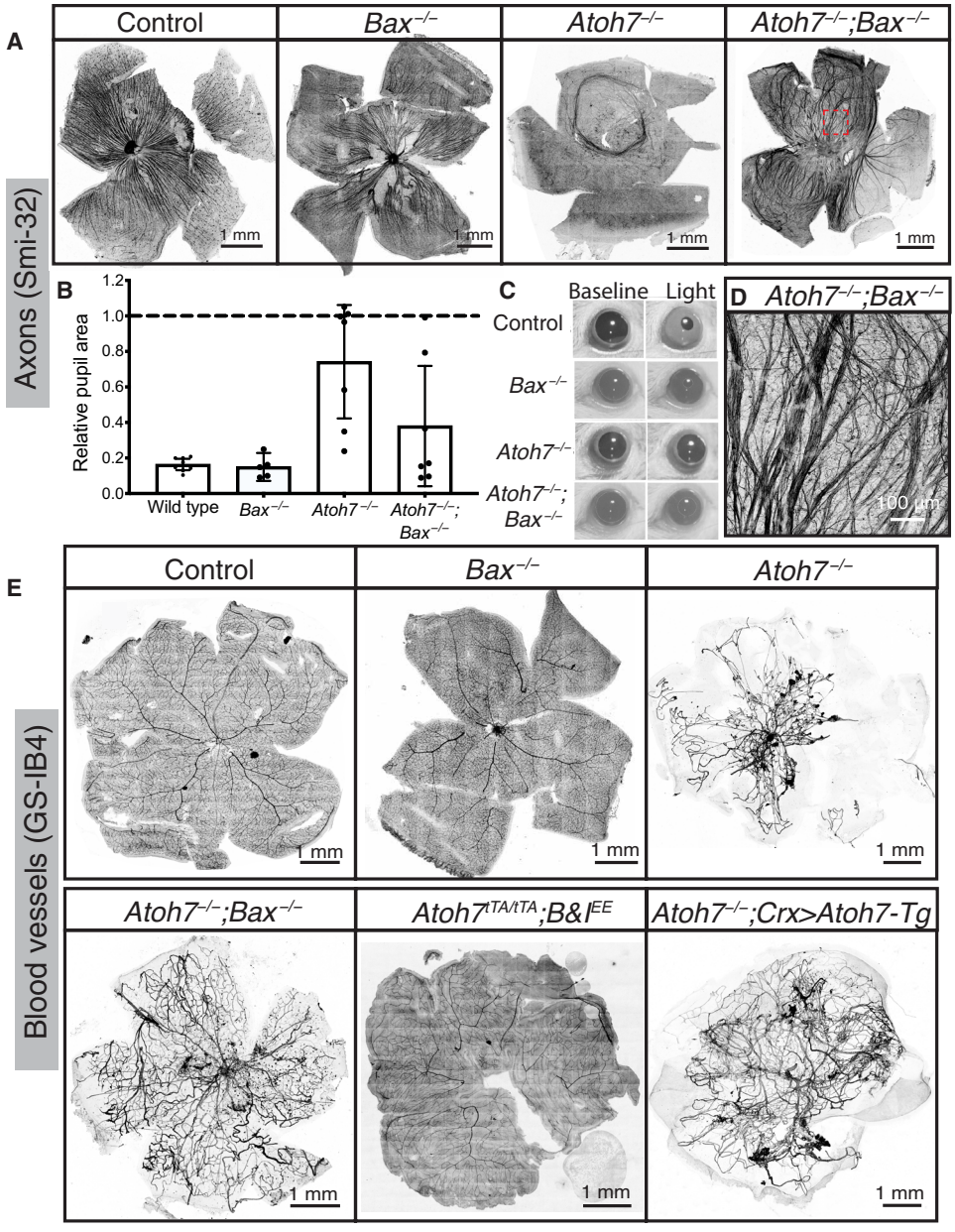

Fig. 3. RGC axon guidance and retinal vasculature development require Atoh7-dependent RGCs. (**A** and **D**) Smi-32 labels a subset of RGCs and their axons in an adult WT retina. In *Atoh7*$^{-/-}$ mice, the Smi-32–positive RGCs have axon guidance deficits. In *Atoh7*$^{-/-}$;*Bax*$^{-/-}$ mice, RGCs have severe axon guidance deficits. Highlighted region (A, *Atoh7*$^{-/-}$;*Bax*$^{-/-}$) is magnified in (D). (**B** and **C**) Using the contralateral PLR as a readout of retina to brain connection allows the appreciation that the severe axon guidance deficits allow for some connection to the brain of the RGCs in the *Atoh7*$^{-/-}$ or *Atoh7*$^{-/-}$;*Bax*$^{-/-}$ retinas. (**E**) It has been previously reported that the hyaloid vasculature fails to regress in *Atoh7*$^{-/-}$ mice, thought to be due to lack of RGCs; however, when the RGC numbers are rescued, in *Atoh7*$^{-/-}$;*Bax*$^{-/-}$mice, the hyaloid vasculature fails to regress. However, *Atoh7* is not necessary for the hyaloid regression and retinal vasculature development, seen using *Atoh7*$^{tTA/tTA}$;*B&I*^{EE} mice, which was previously seen to rescue all of the *Atoh7* null phenotypes. When *Atoh7* is rescued using the *Crx>Atoh7* transgene on the *Atoh7* null background, the optic nerve and 12% of RGCs are rescued (*22*), but the hyaloid vasculature does not regress.

(Fig. 4, A and B, and fig. S11A). Analysis of the cell-type proportions across the genotypes revealed a depletion of RGCs in both *Atoh7* mutant samples (*Atoh7*$^{-/-}$ and *Atoh7*$^{-/-}$;*Bax*$^{-/-}$) compared to both WT and *Bax*$^{-/-}$ controls (Fig. 4, C and D, and fig. S10, E and F). This reduction in the number of RGCs included a compensatory increase in cone photoreceptors and neurogenic RPCs, consistent with previous findings (Fig. 4, C and D, and fig. S10, E and F) (*1*, *8*, *12*, *63*).

Using the scRNA-seq data, we next assessed the differential gene expression within neurogenic RPCs and RGCs across control—WT and *Bax*$^{-/-}$—and *Atoh7*-deficient—*Atoh7*$^{-/-}$ and *Atoh7*$^{-/-}$;*Bax*$^{-/-}$—samples. Using strict differential expression cutoffs (q value < 1×10^{-300}), we identified 230 *Atoh7*-dependent differentially expressed transcripts within neurogenic RPCs and RGCs (table S1). Genes enriched within control samples (Fig. 4E) highlighted many known factors in the specification and differentiation of RGCs, including

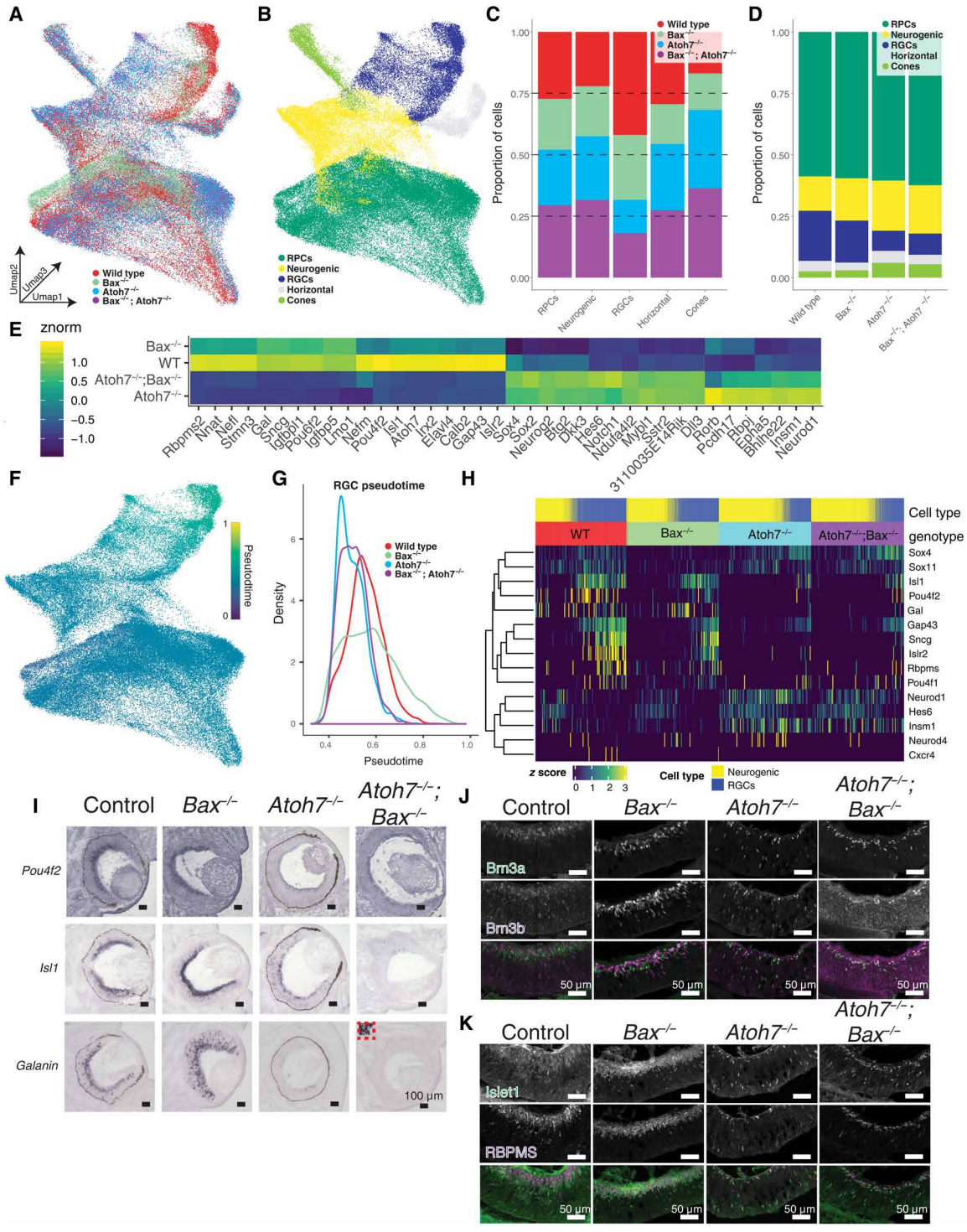

Fig. 4. Single-cell analysis of E14.5 mutant retinas and gene detection in E14 retinas. (**A** and **B**) Uniform manifold approximation and projection (UMAP) dimension reduction of aggregated E14.5 single-cell dataset colored by (A) genotype and (B) annotated cell type. (**C**) Proportions of cell types derived from each genotype. (**D**) Proportions of annotated cell types within each genotype. (**E**) Heatmap of differentially expressed transcripts across control and Atoh7 knockout (*Atoh7*$^{-/-}$ or *Atoh7*$^{-/-}$;*Bax*$^{-/-}$) neurogenic and RGCs. (**F**) UMAP dimension reduction of cells colored by Scanpy pseudotime values. (**G**) Density of RGCs along pseudotime by genotype. (**H**) Heatmap displaying differentially expressed transcripts across the interaction of pseudotime and genotype. Cells are ordered by pseudotime within each genotype. (**I**) Chromogenic in situ hybridization detecting RNA transcripts of genes from (H). Inset, depicted by red dotted lines, *Atoh7*$^{-/-}$;*Bax*$^{-/-}$ mice in (H) show robust galanin signal in a region outside the retina but minimal signal in the retina (**J** and **K**). Immunohistochemistry detecting (J) RGC-specific markers, BRN3A and BRN3B, and (K) pan-RGC markers, ISL1 and RBPMS, in E14 retina from each genotype. Scale bars, 50 μm. RPCs, retinal progenitor cells; RGCs, retinal ganglion cells.

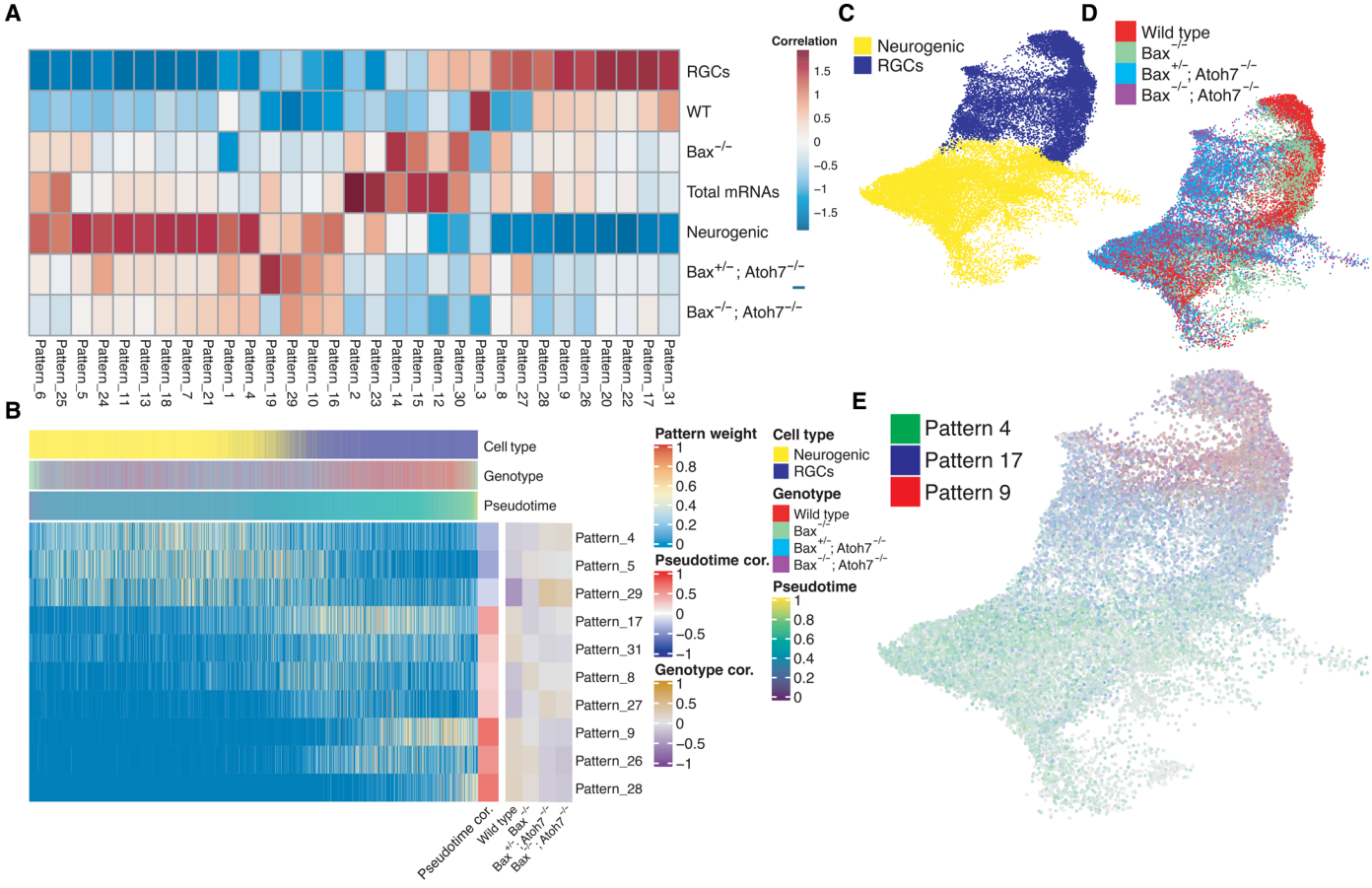

Fig. 5. scCoGAPS analysis of single-cell dataset and RGC population changes in E12.5 retinas show a developmental delay in *Atoh7*$^{-/-}$;*Bax*$^{-/-}$ mutants. (**A**) Heatmap showing the correlation between scCoGAPS pattern and cellular features. (**B**) Heatmap of pattern weights within individual cells ordered by pseudotime. Pattern correlations with both pseudotime and each genotype are displayed on the right. (**C** to **E**) UMAP embedding of single-cell dataset used for scCoGAPS and colored by (C) cell type or (D) genotype. (E) UMAP embedding of dataset and colored by pattern weights of scCoGAPS patterns 4, 17, and 9, displaying progressive pattern usage across RGC development.

Pou4f2 (*Brn3b*), *Isl1*, *Pou6f2* (*Rpf-1*), *Elavl4*, *Gap43*, and *Irx2* (fig. S11B) (*64*–*67*). Conversely, differentially expressed transcripts enriched in the *Atoh7* knockout samples (Fig. 4E) were enriched for genes involved in the Notch signaling pathway—*Rbpj*, *Dll3*, *Notch1*, and *Hes6*—and for transcripts enriched in neurogenic cells and photoreceptor precursors during retinal development—*Btg2*, *Neurog2*, *Bhlhe22*, *Insm1*, *Neurod1*, *Mybl1*, *Sstr2*, and *3110035E14Rik* (fig. S11B) (*23*).

Atoh7-deficient RGCs also show dramatically reduced expression of genes known to regulate axon guidance, including the cell adhesion molecule *Islr2*, which has been found to control RGC axon fasciculation, as well as axon guidance at the optic chiasm (*68*). Of particular interest are the observed increases in *Rbpj* and *3110035E14Rik* expressions in *Atoh7*$^{-/-}$ and *Atoh7*$^{-/-}$;*Bax*$^{-/-}$ samples. *Rpbj* is an upstream regulator of *Atoh7* expression (*69*) and *3110035E14Rik* (*Vxn*), which functions similarly to Atoh7 by promoting retinal neurogenesis and early retinal cell fate specification (*70*). The increased expression of transcripts that show enriched expression in neurogenic cells and photoreceptor precursors is consistent with the increase in generation of cone photoreceptor precursors seen in *Atoh7*-deficient retinas (Fig. 4D) (*1*). Combined with a recovery in the specification of RGC numbers in adult *Atoh7*$^{-/-}$;*Bax*$^{-/-}$ animals, these data suggest that loss of *Atoh7* expression leads to an increase in expression of genes specific to neurogenic RPCs at the expense of RGC-enriched transcripts; results are consistent with a developmental delay.

As albino mice are known to have fewer ipsilaterally projecting RGCs (*71*) and because *Bax*$^{-/-}$ mice are on an albino background, we specifically examined the expression of transcripts traditionally down-regulated in albino mice. Most of these transcripts are down-regulated in *Bax*$^{-/-}$ retinas at E14.5; however, these ipsilateral transcripts were similar to WT in both *Atoh7*$^{-/-}$ *and Atoh7*$^{-/-}$;*Bax*$^{-/-}$ E14.5 retinas (fig. S11C) (*71*), suggesting that the albino background does not contribute to the observed phenotypes in Atoh7$^{-/-}$;Bax$^{-/-}$ mice.

Pseudotemporal analyses identify changes in Atoh7-dependent gene expression during RGC specification

To further assess the degree of an RGC-specific developmental delay, we performed pseudotemporal analyses using Scanpy (Fig. 4F) (*72*). We observed bias of the *Atoh7*-deficient cells within early pseudotime stages during RGC differentiation. Both WT and *Bax*$^{-/-}$ control cells had a broader distribution of cells across pseudotime;

results are consistent with a failure of maturation or developmental delay of RGC specification in *Atoh7*-deficient RGCs (Fig. 4G). Differential expression analysis assessing for differences between the genotypes' pseudotemporal gene expression dynamics revealed significant genotypic differences across RGC development (Fig. 4H and table S2).

In both *Atoh7*$^{-/-}$ and *Atoh7*$^{-/-}$;*Bax*$^{-/-}$ samples, we observed a reduction of expression in many genes enriched within mature RGCs—*Pou4f2*, *Gap43*, *Sncg*, *and Isl1*. We likewise observed reduced expression of a subset of genes in neurogenic RPCs, including *Gal*. Increased expression of other genes predominantly expressed in neurogenic RPCs, including *Neurod1*, *Insm1*, *Neurod4*, *Hes6*, *Onecut1*, *Onecut2*, and *Sox4*, is observed in both *Atoh7*-deficient neurogenic RPCs and RGCs compared to controls (Fig. 4H). This implies that loss of function of *Atoh7* may delay the differentiation of RGCs from neurogenic RPCs. The temporal expression patterns of genes involved in RGC specification mimic those observed within additional E14 scRNA-seq datasets (*62*), and analyses of transcriptomic changes resulting from loss of *Atoh7* expression closely match those obtained from scRNA-seq–based analysis of *Atoh7*$^{-/-}$ retina conducted at E13.5 (*73*).

We next performed in situ hybridization to examine changes in global transcript expression within the developing retina. RNA transcript expression was detected at E14.5, at which point most RGCs are specified (*19*, *20*), and we observed decreased expression of *Pou4f2* (*Brn3b*), *Isl1*, and *Gal* in both *Atoh7*$^{-/-}$ and *Atoh7*$^{-/-}$;*Bax*$^{-/-}$ mice, as determined by chromogenic in situ hybridization (Fig. 4I). Immunostaining of E14 retinas confirms a reduction in the number of cells immunopositive for Brn3a (Pou4f1) and Brn3b (Pou4f2) (Fig. 4J), as well as the pan-RGC markers RBPMS and Isl1 (Fig. 4K), in the developing GCL of *Atoh7*-deficient retinas. At E12.5, we observed a marked decrease in both overall RGC density and RGC number (fig. S8). Together, these results suggest that loss of function of *Atoh7* delays RGC differentiation and leads to an accumulation of neurogenic RPCs.

To further identify patterns of temporal changes in gene expression across RGC genesis between *Atoh7* mutant and control retinas, we performed the nonnegative matrix factorization analysis of the Bayesian NMF technique Single Cell Coordinated Gene Activity in Pattern Sets (scCoGAPS) (*74*). Implementation of scCoGAPS parses the gene expression into groups ("patterns") based on gene expression profiles without a priori, literature-based knowledge of gene interactions. Using 5235 highly variable genes across the 29,182 neurogenic RPCs and differentiating RGCs, we identified 31 patterns of gene expression (Fig. 5, A, B, and E, and fig. S12). These patterns correlated with both neurogenic RPC—patterns 6, 25, 5, 24, 11, 13, 18, 7, 21, 1, and 4—and RGC—patterns 8, 27, 28, 9, 26, 20, 22, 17, and 31—cell-type annotations and highlighted temporal changes in gene expression, as assessed through pseudotime analyses (Fig. 5, A, B, and E). Individual patterns, patterns 4, 5, and 29, were highly correlated with neurogenic cell annotations and *Atoh7*$^{-/-}$ and *Atoh7*$^{-/-}$;*Bax*$^{-/-}$ genotypes, consistent with a temporal delay in RGC specification, increased number of neurogenic cells, or failure of cell-type specification of neurogenic RPCs as a consequence of lost *Atoh7* expression (Fig. 5, A, B, and E). Genes driving pattern 5 include genes enriched in early-stage neurogenic RPCs, *Gadd45a* and *Sox11* (*23*).

Conversely, patterns highly correlated with RGC cell-type annotations and pseudotime—patterns 9, 26, and 28—had a high correlation with control samples (Fig. 5, A, B, and E). The most highly weighted genes in patterns 9 and 26 are *Gap43* and *Igfbpl1*, respectively, which have been implicated in RGC axonal growth (*75*, *76*). Pattern 28 highlights cells toward the end of the RGC trajectory and is largely driven by Sncg, a transcript enriched in most RGCs in the adult mouse retina (Fig. 5, A and B) (*77*). The association of neurogenic patterns with *Atoh7*$^{-/-}$ mutant retinas versus those that highlight RGC differentiation and maturation patterns with control retinas further support a developmental delay in mutant RGCs. Analysis of pattern marker expression across the genotypes (fig. S12) highlights both the temporal delay and global changes in gene expression across the *Atoh7*$^{-/-}$ mutant retinas compared to controls.

Recent studies have comprehensively profiled RGC subtype diversity in the mouse retina (*78*, *79*). However, these studies did not characterize either the birthdates of individual RGC subtypes or the transcriptional networks controlling RGC subtype specification. The delay in RGC maturation and the failure of optic nerve formation seen in *Atoh7*-deficient retinas suggest that the earliest pathfinding RGCs are *Atoh7* dependent. We examined expression of markers of mature RGC subtypes (*78*) within the developing retina and correlated expression of the transcripts with RGC pseudotime (fig. S13), as many of the mature RGC subtype markers are not specific to RGCs. We detected expression of selective markers for a fraction of mature RGC subtypes within the E14.5 scRNA-seq dataset. Of transcripts in which readily detectable expression was observed, many—including *Igfbp4*, *Foxp1*, *Stxbp6*, *Bhlhe22*, and *Penk*—also display enriched expression in primary or neurogenic RPCs. Expression of some markers of RGC development and maturation—*Ebf3*, *Pou4f1*, *Pou4f2*, *Prdm8*, and *Slc17a6*—correlated well with pseudotemporal ordering and were depleted in *Atoh7*-deficient RGCs. However, a limited number of RGC subtype markers, including *Irx3*, *Calb2*, and *Tac1*, were largely absent from *Atoh7* mutant RGCs.

Atoh7 binds to loci associated with neurogenic RPC, RGC, and photoreceptor-enriched genes

To gain insight into the function of Atoh7 during RGC specification, we performed Cut&Run experiments (*80*) on E14 mouse retinas using the established Atoh7 antibody (*27*) and immunoglobulin G (IgG) as a control. Peak calling was performed using the MACS2 pipeline (*81*). High concordance of called peaks is observed between Atoh7 Cut&Run replicates (fig. S14A), with >3000 shared peaks and little enrichment of peak sequences within the IgG sample. Comparisons of Atoh7 peaks to developmental chromatin accessibility (*82*) determined that peaks proximal to gene transcription start sites, corresponding to proximal promoters, exhibited high accessibility throughout retinal development (fig. S14B). Distal peaks, corresponding to enhancer sequences (>3 kb from the transcription start sites), however, displayed the greatest accessibility during early periods of retinal development when RGCs are being generated and when Atoh7 expression is maximal (fig. S14B) (*27*). We next determined the enrichment of DNA sequence motifs underneath called peaks using HOMER (*83*). We observed a highly enriched motif (CAGCTG; $P = 1 \times 10^{-763}$) that was present within >55% of called peaks (13.75% of background peaks; Fig. 6A and table S3). Analysis of motif similarity to known transcription factor motifs indicated a high similarity of the called Atoh7 motif to the Atoh1 motif (CAGCTG; $P = 1 \times 10^{-784}$; Fig. 6A) and other E-Box transcription factors (table S4).

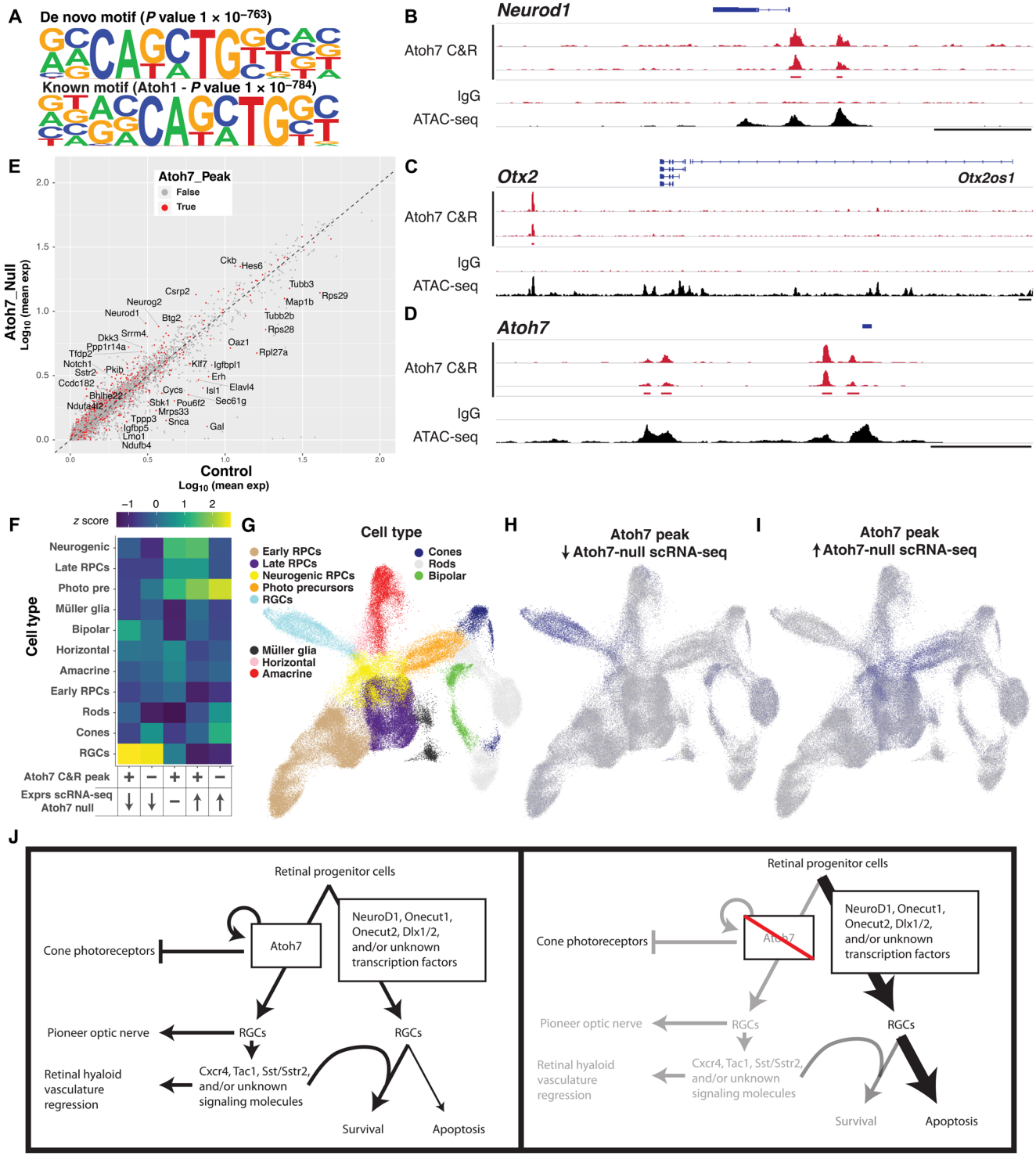

Fig. 6. Cut&Run analysis of Atoh7 genomic binding identifies transcriptional targets of Atoh7. (**A**) HOMER motif analysis of most significant de novo (top) enriched motifs within peaks and similarity of enriched motifs to established transcription factor motifs (bottom). (**B** to **D**) Atoh7 and IgG Cut&Run sequencing tracks within the (B) *Neurod1*, (C) *Otx2*, and (D) Atoh7 genomic loci. Additional E14 ATAC-seq tracks (*82*) show the alignment of Atoh7 Cut&Run peaks with open chromatin. (**E**) Average expression of transcripts within the control (WT and $Bax^{-/-}$) and Atoh7 null ($Atoh7^{-/-}$ or $Atoh7^{-/-}$;$Bax^{-/-}$) neurogenic RPCs and RGCs. Transcripts with Atoh7 Cut&Run peaks are indicated in red. Gene names are displayed for transcripts that display both Atoh7 Cut&Run peaks and high residual to the mean. (**F**) Cellular enrichment of transcript expression within the developmental scRNA-seq dataset (*23*) of genes with the presence/absence of Atoh7 binding and increased, decreased, or no change in expression within *Atoh7* mutant neurogenic RPCs and RGCs compared to control cells. (**G** to **I**) UMAP dimension reductions of the developmental scRNA-seq dataset (*115*) displaying the annotated (G) cell types or (H and I) normalized cellular *z* scores of (H) Atoh7-bound transcripts with decreased or (I) increased expression in *Atoh7* mutants. (**J**) Model showing the role of Atoh7 in retinal development based on the findings of this study.

We next assigned peaks to genes using ChiPSeeker (*84*). Many strong peaks were located within genetic loci of transcripts with known functions during early retinal development, including *Neurod1*, *Elavl4*, *Neurog2*, *Pou6f2*, *Otx2*, *Meis2*, and *Lhx4* (Fig. 6, B to E, and table S5). We also observed strong enrichment of Atoh7 binding within the *Atoh7* proximal promoter and distal enhancer sequences (*14*), suggestive of autoregulation of *Atoh7* expression (Fig. 6D). In addition, we detected Atoh7 binding within numerous loci associated with RGCs, including *Rbpms*, *Pou4f2*, *Isl1*, and *Pou4f1* (fig. S14, C to F, and table S5); however, the binding sites of Atoh7 within the *Pou4f2* locus are located within the intron of the neighboring gene *Ttc29* and, therefore, are assigned to *Ttc29* instead of *Pou4f2*.

To better understand the mechanism by which Atoh7 regulates transcription of nearby genes, we next examined the consequence of *Atoh7* loss of function on bound loci gene expression, as determined by our scRNA-seq experiments in control (WT and $Bax^{-/-}$) versus *Atoh7* null ($Atoh7^{-/-}$ and $Atoh7^{-/-};Bax^{-/-}$) neurogenic cells and RGCs (fig. S15). Our analyses indicated that many Atoh7-bound genes display decreased expression within *Atoh7* mutant retinas, including the RGC-enriched genes *Pou6f2*, *Elavl4*, *Isl1*, and *Tubb2b* (Fig. 6E). Conversely, roughly similar numbers of "bound" genes displayed increased expression in *Atoh7* mutant retinas, including neurogenic RPC-enriched transcripts *Hes6*, *Btg2*, *Neurod1*, *Neurog2*, *Sstr2*, *Pkib*, *and Bhlhe22* (Fig. 6E) (*23*). To gain further insight into the biological relevance of Atoh7-bound and differentially expressed transcripts, we first binned transcripts into five categories: (i) Atoh7-bound and down-regulated in *Atoh7* mutants, (ii) Atoh7-bound and up-regulated in *Atoh7* mutants, (iii) no binding and down-regulated in *Atoh7* mutants, (iv) no binding and up-regulated in *Atoh7* mutants, and (v) Atoh7-bound but no change in expression. Following binning, we calculated the *z* scores of gene expression on an individual cell basis using the mouse retinal development single-cell dataset (*23*) and examined the enrichment of expression of binned genes within annotated cell types. Our analysis determined that Atoh7-bound genes that displayed decreased expression in *Atoh7* mutant retinas show enriched expression in RGCs, suggesting an active role of Atoh7 in promoting RGC fate (Fig. 6, F to H). Conversely, Atoh7-bound genes that are up-regulated in *Atoh7* mutant retinas display high expression within neurogenic cells or photoreceptor precursors and include *Neurod1*, *Neurog2*, and *Hes6* (Fig. 6, F and I). We also observe Atoh7 binding within additional cone photoreceptor gene loci, including *Lhx4*, *Otx2*, and *Thrb* (table S5), although these genes did not display robust differences in gene expression between control and *Atoh7* mutant retinas. The up-regulation of Atoh7-bound neurogenic and photoreceptor-enriched genes in *Atoh7* mutant retinas suggest that Atoh7 actively represses photoreceptor fate during early retinogenesis, an interpretation that is supported by the observed modest increase in cone photoreceptor proportions within *Atoh7* mutant scRNA-seq samples (Fig. 4D).

Galanin is not the Atoh7-dependent secreted factor that promotes RGC survival and pathfinding

Our data suggest the existence of Atoh7-dependent factors that promote both RGC survival and pathfinding, as well as hyaloid vascular regression, in a non–cell-autonomous manner. These are likely derived from Atoh7-expressing neurogenic RPCs and/or RGCs. Factors mediating hyaloid regression are likely to be secreted, while those regulating RGC survival could also potentially act through contact-mediated signaling. Few annotated secreted proteins show clear Atoh7-dependent expression in our scRNA-seq dataset. The neuropeptide galanin (*Gal*), which is strongly expressed in both neurogenic RPCs and RGCs and is a direct target of Atoh7 (Fig. 6E), was by far the most differentially expressed secreted factor in *Atoh7*-deficient mice (Fig. 4, E and I; Fig. 6E; and table S1). Galanin has been implicated in promoting the survival of neural precursors (*85*, *86*) and to be enriched in ipsilaterally projecting RGCs (*62*). However, *Gal*-deficient animals showed no differences in either the hyaloid vasculature regression or RGC density, as compared to the control animals (fig. S16).

DISCUSSION

It is broadly accepted that Atoh7 acts in RPCs as a competence factor that is essential for RGC specification (*10*, *39*, *40*, *87*). In this study, though, we show that the specification of the great majority of RGCs occurs even in the absence of *Atoh7*. While RGC specification can occur independent of Atoh7, Atoh7 function is required to maintain RGC survival and proper targeting of RGC axons to the optic nerve head (Fig. 6J). Following disruption of both *Atoh7* and *Bax*, we observe only a 20% reduction in the number of RGCs relative to *Bax*-deficient controls. This compares to a greater than 95% reduction in RGC numbers in *Atoh7* mutants relative to WT controls. Although RGCs in $Atoh7^{-/-};Bax^{-/-}$ retinas show severe defects in targeting the optic nerve head, they respond robustly to photoreceptor stimulation.

The presence of functional RGCs in the absence of Atoh7 helps explain long-standing, puzzling observations: (i) 45% of RGCs are not derived from *Atoh7*-expressing progenitors, (ii) molecular markers of RGCs are observed at considerably higher levels during early stages of retinal development than in adults in Atoh7-deficient retinas, and (iii) the marked increase in apoptosis in the GCL that occurs in the absence of Atoh7 (*10*, *22*, *25*). Previous studies have implicated Atoh7 as a direct upstream regulator of the essential RGC transcription factors *Brn3a*, *Brn3b*, and *Isl1*. Supporting this, an *Atoh7* hierarchy of RGC determinants, studies in which *Brn3b* and *Isl1* were inserted in place of the *Atoh7* coding sequence observed a complete rescue of normal RGC development (*37*). Our studies, however, indicate that when apoptosis is inhibited, Brn3a, Brn3b, Islet1, and Rbpms expression is induced at near-normal levels within RGCs in both E14 and adult retinas, independent of *Atoh7* expression. We observe that Atoh7 binds to sites in the *Isl1* and *Pou4f1* (Brn3a) loci (fig. S14, E and F), suggesting active regulation of *Isl1* and *Brn3a* transcription by Atoh7. While no Atoh7 Cut&Run peak was assigned to *Pou4f2* (*Brn3b*), two Atoh7-binding sites were identified in the terminal intron of *Pou4f2*-neighboring gene *Ttc29* (fig. S14D). While further evidence is required to clearly demonstrate that Atoh7 regulates *Pou4f2* expression via these binding sites, we observed reduced expression of *Isl1*, *Pou4f1*, and *Pou4f2* within Atoh7-deficient retinal cells. Therefore, we conclude that other factor(s) in addition to Atoh7 activate expression of these genes.

The molecular mechanisms by which *Atoh7* controls axonal guidance and cell survival remain unclear. One hypothesis is that RGC axonal guidance and cell survival are linked and that loss of *Atoh7* expression fails to initiate expression of target-derived trophic cues. Because other studies have failed to detect substantial numbers of RGCs in $Atoh7^{-/-}$ mice at postnatal day 0 (P0) (*1*, *8*, *22*, *25*) and target-derived neurotrophic factors regulate apoptosis of RGCs between P0 and P12, we suspect that Atoh7-regulated prosurvival factors act at earlier time points than target-derived trophic signals. In addition,

as we did not observe RGC rescue within *Atoh7*$^{Cre/Cre}$;*Bax*$^{fl/fl}$ mice, we suggest that immature RGCs rapidly degenerate as the result of the lack of an Atoh7-dependent survival factor. This wave of developmental apoptosis has been observed previously, but the underlying molecular mechanisms are unknown (*46*, *47*, *88*–*92*). We hypothesize that this prosurvival factor or factors must be produced by either *Atoh7*-expressing neurogenic RPCs or RGCs derived from these cells.

Our data also reveal a marked delay in the formation of RGCs from neurogenic RPCs in the absence of *Atoh7*. This is consistent with previous results in *Atoh7*$^{-/-}$ retinas, where RGC formation is delayed by at least a day, in part due to RPCs remaining in cell cycle (*22*, *93*). However, this delay in cell cycle exit later resolves, as essentially normal levels of all other early-born cell types in the *Atoh7*$^{-/-}$;*Bax*$^{-/-}$ retinas, including RGCs (Fig. 1 and fig. 4). When Atoh7-dependent RGCs are rescued later in development, as seen in targeted mutants in which *Atoh7* is expressed from the endogenous *Crx* locus, the hyaloid vasculature regression was not rescued, even though a modest rescue of RGC formation is observed (*22*). Consistent with this result, loss of function of *atoh7* in early-stage RPCs in the zebrafish retina disrupts the correct targeting of axons in later-born RGCs to the optic nerve (*33*). Together with the fact that 45% of RGCs arise from a non–Atoh7-dependent lineage in mice, we hypothesize that early, pathfinding RGCs are Atoh7 dependent and provide both survival and guidance cues for later-born RGCs.

Since *Atoh7* was previously thought to be a master transcriptional regulator of RGC specification, strategies aimed at targeted differentiation of RGCs for therapeutic purposes have focused on using the forced expression of *Atoh7*. We, however, now appreciate RGC specification to be a far more complicated process. Although ectopic expression of *Atoh7* activates expression of RGC-specific genes in cultured RPCs (*94*), induced pluripotent stem cells (*95*), and Müller glia-derived retinal stem cells (*96*, *97*), it is, nonetheless, typically not sufficient to drive these cells to become RGCs. This study sheds light on why this may be the case.

These findings demonstrate that additional factors act in parallel to *Atoh7* to control RGC specification. While multiple other transcription factors have been reported to regulate RGC specification, including *Neurod1*, *Sox4*, and *Onecut2* (*35*, *98*, *99*), these factors are unable to individually activate expression of *Brn3b* and *Isl1*. In *Atoh7*$^{-/-}$;*Bax*$^{-/-}$ RGCs, however, we observe substantially increased expression of each of these transcription factors (Fig. 4E and fig. S12), suggesting the possibility that these factors, among others, may compensate for the loss of *Atoh7*. The observations that Atoh7 binds to target sites in the genomic loci of multiple genes that are up-regulated in *Atoh7* mutant retinas, including *Neurod1*, *Neurog2*, *Otx2*, *and Onecut2*, suggest that Atoh7 directly inhibits alternate mechanisms of RGC genesis. However, the identity of the non–cell-autonomous cues by which *Atoh7* regulates RGC survival, axon guidance, and hyaloid vasculature regression remains unknown (Fig. 6J). Further identification of the mechanisms regulating the interplay of intrinsic and extrinsic signals on RGC specification, survival, and maturation will help guide the future design of therapies aimed at maintaining and replacing RGCs lost due to degenerative disease.

MATERIALS AND METHODS

Mice

Animals were housed and treated in accordance with NIH (National Institutes of Health) and IACUC (International Animal Care and Use Committee) guidelines, and we used protocols approved by the Johns Hopkins University Animal Care and Use Committee (protocol number MO16A212). *Atoh7*$^{Cre/Cre}$ mice are a knock-in line where Cre recombinase replaced the entire *Atoh7* gene and was a gift from L. Gan (referred to as *Atoh7*$^{-/-}$) (RRID:MGI:3717726) (*40*). The Bax$^{tm1Sjk/tm1Sjk}$ (*Bax*$^{-/-}$) mice containing a neomycin cassette that replaces critical exons 2 to 5 were purchased from the Jackson Laboratory (JAX:002994, RRID:IMSR_JAX:002994) (*43*). The *Bax*$^{-/-}$ mice are unpigmented since the *Bax* gene is linked to the *Tyrosinase* (Tyr) and *Pink-eyed dilution* (*p*) gene by 21 and 5 cM, respectively. The conditional Bax$^{tm2Sjk/tm2Sjk}$ (Bax$^{fl/fl}$) mice containing LoxP sites flanking exons 2 to 4 were purchased from the Jackson Laboratory (JAX:006329, RRID:IMSR_JAX:006329) (*100*). *Atoh7*$^{tTA/tTA}$;B&I-EE mice are a combination of two genetic strains. In the first strain (*Atoh7*$^{tTA/tTA}$), the tetracycline-responsive artificial transcription factor tTA replaces the *Atoh7* gene. In the absence of tetracycline, the tTA activates the tetracycline-responsive element that is driving the expression of *Brn3b* and *Isl1* in the second strain (B&I-EE). Therefore, in effect, the Atoh7 promoter will drive the expression of *Brn3b* and *Isl1*. This mouse line has been previously reported to rescue all reported effects of *Atoh7* loss of function and was a gift from X. Mu (MGI:5749708 and MGI:5749713) (*37*). The *Crx>Atoh7* mice, a transgene that expresses the full-length *Atoh7* coding sequence under the control of the *Crx* promoter, was previously published (MGI:5433215) (*22*). A tdTomato Cre recombinase reporter mouse*Rosa26*^{tdTomAi14} (JAX:007914, RRID:IMSR_JAX:007914) (*101*) was used to label cells in a Cre recombinase–dependent manner. The *Chx10-Cre* mouse line is a transgenic line purchased from the Jackson Laboratory, originally developed by C. Cepko's laboratory (JAX:005105, RRID:IMSR_JAX:005105) (*52*), and expresses Cre recombinase broadly in all RPCs from E10 to E15.5. The *Opn4*^{taulacZ} mice were used to trace the ipRGC projections to the brain (*55*). Throughout the manuscript, controls are heterozygous for both *Atoh7* and *Bax* (*Atoh7*$^{+/-}$;*Bax*$^{+/-}$), whereas *Atoh7*$^{-/-}$ mice were also heterozygous for *Bax* (*Atoh7*$^{-/-}$;*Bax*$^{+/-}$).

Statistics

All statistical tests, apart from analysis of the scRNA-seq data, were performed in GraphPad Prism 6 (RRID:SCR_002798). The statistical tests used are listed in figure captions.

Immunohistochemistry

Adult retinas from P40 to P200 mice were obtained by enucleating whole eyes, fixing for 30 min in 4% paraformaldehyde (PFA) diluted in phosphate-buffered saline (PBS), dissecting to remove the cornea and lens, and dissecting the retina from the RPE, and antibody staining proceeded in a 24-multiwell cell culture plate (Corning, no. 353047). Retinas were blocked in 500 µl of PBS containing 0.3% Triton X-100 and 6% goat serum for 2 hours at room temperature (RT). Several antibodies were used in this study (dilutions are in parentheses): Mouse IgG1 anti-Brn3a (Millipore, catalog no. MAB1585, RRID:AB_94166) (1:250), Rabbit anti-RBPMS (GeneTex, catalog no. GTX118619, RRID:AB_10720427) (1:250), Rabbit anti-Brn3b (1:100) (*49*, *102*), Mouse anti-Smi32 [nonphosphorylated anti–neurofilament H (NF-H)] (BioLegend, catalog no. 801701, RRID:AB_2564642) (1:500), Mouse anti-neurofilament medium (Thermo Fisher Scientific, catalog no. 13-0700, RRID:AB_2532998) (1:500), Chicken anti-neurofilament heavy (Millipore, catalog no. AB5539, RRID: AB_11212161) (1:250), Mouse anti-GFAP (Sigma-Aldrich, catalog

no. C9205, RRID:AB_476889) (1:1000), GS-IB4 (Molecular Probes, catalog nos. I21411 and I21411, RRID:AB_2314662) (1:250), Rabbit anti-Pax2 (BioLegend, catalog no. 901001, RRID:AB_2565001) (1:100), Mouse anti-Tuj1 (R&D Systems, catalog no. MAB1195, RRID:AB_357520) (1:200), Rabbit anti-DsRed (Takara Bio, catalog no. 632496, RRID:AB_10013483) (1:250), Mouse anti-Islet1 (DSHB, catalog no. 40.2D6, RRID:AB_528315) (1:200), and Rabbit anti-Opn4 (Advanced Targeting Systems, catalog no. UF006, RRID:AB_2314781) (1:500), Rabbit anti-Pax6 (Millipore, catalog no. AB2237, RRID:) (1:500), Mouse anti-Rxrgamma (Santa Cruz Biotechnology, catalog no. sc-365252, RRID:AB_10850062) (1:200), Rabbit anti-Cone arrestin (Millipore, catalog no. AB15282, RRID:AB_1163387) (1:1000), and Mouse anti-calbindin (Sigma-Aldrich, catalog no. C9848, RRID:AB_476894) (1:1000). The appropriate antibodies were diluted in blocking solution and incubated for 2 days at 4°C. Retinas were then washed in three changes of PBS, 15 min each, and then placed in the appropriate Alexa Fluor secondary antibody (1:500; Invitrogen) overnight at 4°C. Retinas were washed in 200 µl of PBS containing 1× DAPI (4′,6-diamidino-2-phenylindole), then washed three times in PBS for 15 min each, and mounted flat on slides in VectaShield (Vector Labs, RRID:AB_2336789). Regionalized dissections were done as follows: Before enucleation, the most nasal part of the sclera was marked with a cauterizer. This mark was used during the dissection to make a marking incision into the retina, following the above staining protocol. Retinas were imaged on a Zeiss LSM 700 or 800 confocal microscope at the Johns Hopkins University Integrated Imaging Center Core Facility (RRID:SCR_016187).

For embryonic studies, developing embryos harvested at E12.5 and E14.5 were washed in a petri dish with sterile PBS three times for 10 min. Tail was used for genotyping. The heads were fixed in 4% PFA for 30 min and then cryoprotected in 30% sucrose at 4°C overnight, frozen in optimal cutting temperature compound (OCT), and sectioned at 18-µm thickness using a cryostat. Sections were dried at 30°C for 15 min and then washed for 10 min in three changes of PBS. Sections were then blocked and stained as above in a humidified chamber overnight. Sections were then mounted and imaged as described.

Cell density analysis

All cell counting was done manually. To confirm the reproducibility of the cell counts, randomly selected selections from each sample were counted twice, and counts were consistently found to be essentially identical. Density was calculated as the number of cells per area. All measurements and cell number analysis were done manually in ImageJ (Fiji, RRID:SCR_002285) and Adobe Photoshop CS6 (RRID:SCR_014199).

In adult flat-mounted retinas, the density of RGCs was calculated by obtaining at least four representative images at 40× of 600 µm × 600 µm with 1-µm optical sections. Optical sections were projected together with maximum intensity, including cells only in the retinal layers of interest. Representative images were taken similarly across all genotypes without a priori knowledge of the genotype. However, some genotypes contain marked phenotypic differences, which include a pigment mutation linked to the *Bax* locus, drastic RGC number reduction as in the *Atoh7*$^{-/-}$, and/or misguided axons. Three representative areas of each retina were averaged for the density analysis.

In E12.5 embryonic retinal sections, a representative confocal image was taken at 40× of 600 µm × 600 µm with optical sections of 1 µm projected together with maximum intensity. The sections chosen for analysis were all positive for Pax2^{+} optic nerve head cells, as the central retina contains the earliest-born RGCs. At least two sections with matching criteria were analyzed for each E12.5 embryo. Density was calculated by dividing the number of Brn3a^{+} RGCs and dividing by the area of the retina. To limit the analysis to the RGC neurogenic zone, we limited the quantification to the leading edge of RGC genesis. The percentage of mature Brn3a^{+} RGCs at E12.5 was determined by counting their number within the GCL. The number of mature Brn3a^{+} RGCs was then divided by the number of total Brn3a^{+} RGCs in a section and then averaged across all sections. This ratio represents the number of Brn3a^{+} RGCs already in the nascent GCL versus RGCs migrating through the neuroblast layer to the GCL.

MEA recordings

Mice were dark-adapted for 1 to 2 hours before being euthanized and dissected under dim red light. Retinas were isolated in Ames' medium (Sigma-Aldrich) bubbled with 95% O_2/5% CO_2 (carbogen) at RT, trimmed into small rectangles, and then placed on a 6 × 10 perforated MEA (Multichannel Systems, Tübingen, Germany), ganglion cell side down. Tissue was perfused with Ames' bubbled with carbogen and kept at 32°C throughout the experiment. Data acquisition was performed using the MC_Rack software (ALA Scientific Instruments Inc.), at a 50-kHz sampling rate. An offline spike sorter (Plexon Inc.) was used for spike sorting.

Ultraviolet stimuli ($I_{mean} \approx 5 \times 10^3$ photons cm^{-2} s^{-1}, 398 nm) were generated through a modified DLP projector (HP Notebook Projection Companion Projector, model HSTNN-FP01) (frame rate = 60 Hz) and were delivered through an inverted microscope objective. All stimuli were programmed using the Psychophysics Toolbox in Matlab (MathWorks, Natick, MA). Stimuli include the following: (i) 120-s, 1-Hz full-field square-wave flash (100% Michelson contrast); (ii) 10-min Gaussian white noise (GWN) flickering checkerboard (pixel size = 44.77 µm); and (iii) 10-min spatially correlated "cloud" stimulus that was generated by low-pass filtering the GWN. The cloud stimulus introduced dark and bright areas of a range of scales within each frame, with the purpose of driving large spatial receptive fields.

The analysis was first performed using custom-written Matlab (MATLAB R2014b) codes; the results later were exported and edited in Adobe Illustrator CS6. For each cell, the PSTH of responses to square-wave flash was calculated using 10-ms bins. Spatial and temporal receptive fields were identified on the basis of noise data using a nonlinear model previously described in detail (*58*, *103*).

Fewer cells were recorded from *Atoh7*$^{Cre/Cre}$;*Bax*$^{-/-}$ mice compared to the WT and *Bax*$^{-/-}$, as the nerve fiber layer (NFL) and retinal vasculature are improperly developed and, thus, provide an insulating layer that needs to be removed in order to obtain high-quality recordings. No cells were recorded from *Atoh7*$^{Cre/Cre}$ mice due to the >99% reduction in RGC numbers.

Pupillary light response

PLR experiments were performed on mice that were dark adapted for at least 1 hour before any experiment. PLR was measured by gently restraining the mice by hand (without anesthesia) and exposing them to a cool white light LED (light-emitting diode) bulb (6500K, light intensity: 15 W/m^2, MR16, SuperBrightLEDs.com) that was directed at one eye using a gooseneck arm of a dissecting microscope light source. Constriction of the pupil was recorded using a Sony Handycam camcorder (FDRAX33) from either the

contralateral or ipsilateral eye to the light source. The baseline pupil size of each mouse was first recorded for at least 5 s using an infrared light source, following which the white LED bulb was turned on for at least 30 s. Video recordings were analyzed by creating screenshot images in Joint Photographic Experts Group format (jpg) of the pupil before and during light stimulation using VLC media player (www.videolan.org/vlc/). The pupil area was then quantified in ImageJ (Fiji, RRID:SCR_002285). To determine the relative pupil area, pupil size during the light stimulation was divided by pupil size before light stimulation.

Tissue dissociation for generation of single-cell suspensions

Eyes were enucleated from E14 time-pregnant animals and placed directly into ice-cold 1× PBS. Retinas were dissected in cold 1× PBS and then placed into 200 μl of cold HBSS (Hanks' balanced salt solution) per two to three retinas. Tissue dissociation was induced through the addition of an equivalent volume of papain solution [1 ml to 700 μl of reagent grade water, 100 μl of fresh 50 mM L-cysteine (Sigma-Aldrich), 100 μl of 10 mM EDTA, and 10 μl of 60 mM 2-mercaptoethanol (Sigma-Aldrich), with papain added to 1 mg/ml (1:10 dilution of 10 mg/ml papain solution; Worthington)]. The papain-retina mixture was placed at 37°C for 10 min with slight trituration every 2 to 3 min. Enzymatic dissociation was halted through the addition of 600 μl of Neurobasal media and 10% FBS for every 400 μl of dissociation solution. DNA from lysed cells was removed using 5 μl of RNase-free DNase I (Roche) for every 1 ml of dissociated cells and incubated at 37°C for 5 min, followed by slight trituration using a 1-ml pipette. Cells were pelleted after centrifugation [300 RCF (relative centrifugal force) for 5 min at 4°C], followed by resuspension in 2 to 3 ml of Neurobasal media supplemented with 1% FBS. The final solution was passed through a 50-μm filter to remove cellular aggregates and undissociated debris.

10x Genomics sequencing and analysis

scRNA-seq of dissociated retinal cells from E14 *Atoh7*$^{-/+}$;*Bax*$^{-/-}$ and *Atoh7*$^{-/-}$;*Bax*$^{-/-}$ was performed using the 10x Genomics Chromium 3′ v2 platform (PN-120223) (Pleasanton, CA), followed by sequencing using the NextSeq 500 platform with default 10× sequencing parameters [R1, 26 base pairs (bp); R2, 98 bp; i7, 8 bp]. Single-cell analysis of the WT E14 developing mouse retina was obtained from previously reported samples obtained from GEO (GSE118614); data obtained using similar isolation protocols are described previously (*23*).

Gene set usage pattern discovery with scCoGAPS

CoGAPS v.3.5.6 (*74*, *104*) was used to find patterns of gene set usage by neurogenic and retinal ganglion cells. The expression matrix used as input was normalized to 10,000 counts per cell, subsetted down to 5235 most highly variable genes, and $\log_2$-transformed. The CoGAPS parameters used are as follows: singleCell = TRUE, nPatterns = 30, nIterations = 50,000, distributed = single-cell, sparseOptimization = True, seed = 803L, and nSets = 10. The final number of patterns stabilized at 31.

Identification of Atoh7-dependent genes

Data were subsetted down to neurogenic RPCs and RGCs. Monocle's differential gene test was conducted between control (WT and *Bax*$^{-/-}$) and Atoh7 mutants (Atoh7$^{-/-}$ Atoh7$^{-/-}$;Bax$^{-/-}$) using the following parameters:

differentialGeneTest(dat[genes expressed in >=10 cells], fullModelFormulaStr = '~(Atoh7 genotype) + Total_mRNAs', reducedModelFormulaStr = '~Total_mRNAs',cores=4).

Pseudotime analysis between genotypes

Scanpy v1.4 (*72*) was first used to assign diffusion pseudotime values (*105*) to cells in the RGC trajectory. Cell types included in this final dataset were restricted to RGCs, primary RPCs, and neurogenic RPCs. To preprocess the dataset, genes <10 counts were removed, and the expression matrix was normalized to 10,000 counts per cell and log-transformed. Highly variable genes used for ordering were identified using Scanpy's "highly_variable_genes" function with default parameters except flavor = "cell_ranger" and n_top_genes = 3000. Fifty principal components were calculated using default PCA (principal components analysis) parameters with random_state = 123,456. To compute the neighborhood graph with the batch effect of genotype removed, we used BBKNN with batch_key = "Genotype" and neighbors_within batch = 3 (*106*). Ten diffusion components were then computed and used for input to assign diffusion pseudotime values with an RPC cell as root. To find genes differentially expressed between the developmental trajectories of the WT and *Atoh7*$^{Cre/Cre}$;*Bax*$^{-/-}$ genotypes, Monocle's differential gene test (*107*, *108*) was performed in R, on neurogenic RPCs and RGCs of WT and *Atoh7*$^{Cre/Cre}$;*Bax*$^{-/-}$ null genotypes:

differentialGeneTest(dat[genes expressed in >=10 cells], fullModelFormulaStr = '~sm.ns(Pseudotime,df=3)*Genotype+Total_mRNAs', reducedModelFormulaStr = '~sm.ns(Pseudotime, df=3)+Genotype+Total_mRNAs',cores=3).

In situ hybridization

Developing embryos harvested at E14.5 were washed in petri dishes filled with sterile DEPC (diethyl pyrocarbonate)–treated PBS at least three times. The head of the embryo was plunged into OCT and then immediately frozen and stored at −80°C until needed, and the tail was used for genotyping. Sections (20 μm) were taken using a cryostat. Sections were allowed to dry on slides for a few hours and then were stored at −80°C until needed. In situ hybridization was performed as previously described (*109*).

Cut&Run

Five retinas from E14 C57BL6/J embryos were dissected and pooled per biological replicate and processed for Cut&Run as described in (*80*) with a few modifications. All steps were carried out in 0.2 ml of PCR (polymerase chain reaction) tube strips and 22 μl of BioMag Concanavalin A beads (Polysciences, catalog no. 86057-3) suspended in an additional 100 μl per sample of binding buffer [20 mM Hepes (pH 7.9), 10 mM KCl, 1 mM $CaCl_2$, and 1 mM $MnCl_2$]. After two washes, the beads were resuspended in 10 μl per sample of binding buffer using a magnetic rack. Retinas were dissociated by pipetting and centrifuged for 3 min at 300*g* in PBS at RT. Cells were then resuspended in 100 μl of buffer 1 [20 mM Hepes (pH 7.5), 150 mM NaCl, 0.5 mM spermidine, and 1× Millipore Protease Inhibitor Cocktail Set III: catalog no. 539134] at RT. After two washes, cells were resuspended in 100 μl per sample of buffer 1 and incubated with beads for 10 min at RT. Supernatant was discarded, and 50 μl of cold buffer 2 (buffer 1, 2 mM EDTA, and 0.01% digitonin) was used to resuspend the cell/bead mix. Two micrograms of Rabbit anti-Atoh7 (Novus Biologicals, NBP1-88639) and 2 μg of rabbit isotype control IgG (Thermo Fisher Scientific, catalog no. 02-6102)

antibodies were added to the samples and incubated at 4°C overnight. Supernatant was cleared the next day, and the cell/bead mix was gently resuspended in 200 µl of cold buffer 3 (buffer 1 and 0.01% digitonin). After two washes, cell/bead mix was gently resuspended in 50 µl of cold buffer 3. One microliter of 50× pAG-MNase was added to the cell/bead mix and incubated at RT for 10 min. Cold buffer 3 (200 µl) was added to wash the cell/bead mix twice. Supernatant was discarded, and the cell/bead mix was resuspended in 50 µl of cold buffer 3. $CaCl_2$ (100 mM) was added, and the samples were incubated on ice for 30 min. Thirty-three microliters of stop buffer [340 mM NaCl, 20 mM EDTA, 4 mM EGTA, RNase A (50 µg/ml), and glycogen (50 µg/ml)] was added to the cell/bead mix, and the samples were incubated for 10 min at 37°C. Beads were discarded, and the supernatant was used to extract DNA using the Qiagen nucleotide removal kit as per the manufacturer's specifications. DNA was eluted in 20 µl of elution buffer and sent for library preparation. Libraries were prepared per the manufacturer's instructions using the KAPA HyperPrep Kit (Roche) and sequenced using the Illumina HiSeq 4000 sequencing system with 2 × 50 bp of sequencing parameters.

Cut&Run data processing

Paired-end reads were aligned to mm10 with Bowtie2 v2.3.5 under parameters "--local --very-sensitive-local --no-unal --no-mixed--no-discordant --phred33 -I 10 -X 700," as described previously (*110*, *111*). Samtools filtered out alignments with less than a 30 MAPQ score (*112*). Picard v2.0.1 MarkDuplicates removed duplicate reads. MACS2 v2.2.7.1 called peaks with the following parameters: "-t Atoh7_bed -c IgG_bed -f BED -g mm --keep-dup all -p 1e-5 -n output_file" (*81*). bedtools found an overlap between the two replicates' peaks with "intersect -u -a Rep1.narrowPeak -b Rep2.narrowPeak" (*113*). Overlapping peaks aligning to mitochondrial or random chromosomes were removed. Homer v4.11 was used for motif discovery by using "findMotifsGenome.pl" under default parameters (*83*). In ChIPseeker v1.22.1, "annotatePeak" was used to annotate the overlapping peaks with genomic features (*84*). DeepTools v3.1.0 was used to generate bigwig files for visualization (default parameters and bin size of 5 bp) and for coverage heatmaps (*114*).

SUPPLEMENTARY MATERIALS

Supplementary material for this article is available at http://advances.sciencemag.org/cgi/content/full/7/11/eabe4983/DC1

View/request a protocol for this paper from *Bio-protocol*.

REFERENCES AND NOTES

1. N. L. Brown, S. Patel, J. Brzezinski, T. Glaser, Math5 is required for retinal ganglion cell and optic nerve formation. *Development* **128**, 2497–2508 (2001).
2. N. M. Ghiasvand, D. D. Rudolph, M. Mashayekhi, J. A. Brzezinski IV, D. Goldman, T. Glaser, Deletion of a remote enhancer near *ATOH7* disrupts retinal neurogenesis, causing NCRNA disease. *Nat. Neurosci.* **14**, 578–586 (2011).
3. A. P. Jarman, E. H. Grell, L. Ackerman, L. Y. Jan, Y. N. Jan, *Atonal* is the proneural gene for *Drosophila* photoreceptors. *Nature* **369**, 398–400 (1994).
4. K. Khan, C. V. Logan, M. M. Kibbin, E. Sheridan, N. H. Elçioglu, O. Yenice, D. A. Parry, N. Fernandez-Fuentes, Z. I. A. Abdelhamed, A. Al-Maskari, J. A. Poulter, M. D. Mohamed, I. M. Carr, J. E. Morgan, H. Jafri, Y. Raashid, G. R. Taylor, C. A. Johnson, C. F. Inglehearn, C. Toomes, M. Ali, Next generation sequencing identifies mutations in *Atonal homolog 7* (*ATOH7*) in families with global eye developmental defects. *Hum. Mol. Genet.* **21**, 776–783 (2012).
5. C. C. Khor, W. D. Ramdas, E. N. Vithana, B. K. Cornes, X. Sim, W.-T. Tay, S.-M. Saw, Y. Zheng, R. Lavanya, R. Wu, J. J. Wang, P. Mitchell, A. G. Uitterlinden, F. Rivadeneira, Y.-Y. Teo, K.-S. Chia, M. Seielstad, M. Hibberd, J. R. Vingerling, C. C. W. Klaver, N. M. Jansonius, E.-S. Tai, T.-Y. Wong, C. M. van Duijn, T. Aung, Genome-wide association studies in Asians confirm the involvement of *ATOH7* and *TGFBR3*, and further identify *CARD10* as a novel locus influencing optic disc area. *Hum. Mol. Genet.* **20**, 1864–1872 (2011).
6. S. Macgregor, A. W. Hewitt, P. G. Hysi, J. B. Ruddle, S. E. Medland, A. K. Henders, S. D. Gordon, T. Andrew, B. M. Evoy, P. G. Sanfilippo, F. Carbonaro, V. Tah, Y. J. Li, S. L. Bennett, J. E. Craig, G. W. Montgomery, K.-N. Tran-Viet, N. L. Brown, T. D. Spector, N. G. Martin, T. L. Young, C. J. Hammond, D. A. Mackey, Genome-wide association identifies *ATOH7* as a major gene determining human optic disc size. *Hum. Mol. Genet.* **19**, 2716–2724 (2010).
7. L. Prasov, T. Masud, S. Khaliq, S. Q. Mehdi, A. Abid, E. R. Oliver, E. D. Silva, A. Lewanda, M. C. Brodsky, M. Borchert, D. Kelberman, J. C. Sowden, M. T. Dattani, T. Glaser, ATOH7 mutations cause autosomal recessive persistent hyperplasia of the primary vitreous. *Hum. Mol. Genet.* **21**, 3681–3694 (2012).
8. S. W. Wang, B. S. Kim, K. Ding, H. Wang, D. Sun, R. L. Johnson, W. H. Klein, L. Gan, Requirement for *math5* in the development of retinal ganglion cells. *Gene Dev.* **15**, 24–29 (2001).
9. S. Kanekar, M. Perron, R. Dorsky, W. A. Harris, L. Y. Jan, Y. N. Jan, M. L. Vetter, Xath5 participates in a network of bHLH genes in the developing Xenopus retina. *Neuron* **19**, 981–994 (1997).
10. J. A. Brzezinski IV, L. Prasov, T. Glaser, *Math5* defines the ganglion cell competence state in a subpopulation of retinal progenitor cells exiting the cell cycle. *Dev. Biol.* **365**, 395–413 (2012).
11. J. N. Kay, K. C. Finger-Baier, T. Roeser, W. Staub, H. Baier, Retinal ganglion cell genesis requires lakritz, a zebrafish atonal homolog. *Neuron* **30**, 725–736 (2001).
12. J. A. Brzezinski IV, N. L. Brown, A. Tanikawa, R. A. Bush, P. A. Sieving, M. H. Vitaterna, J. S. Takahashi, T. Glaser, Loss of circadian photoentrainment and abnormal retinal electrophysiology in *Math5* mutant mice. *Invest. Opthalmol. Vis. Sci.* **46**, 2540–2551 (2005).
13. R. Wee, A. M. Castrucci, I. Provencio, L. Gan, R. N. V. Gelder, Loss of photic entrainment and altered free-running circadian rhythms in *math5*$^{-/-}$ mice. *J. Neurosci.* **22**, 10427–10433 (2002).
14. J. B. Miesfeld, N. M. Ghiasvand, B. Marsh-Armstrong, N. Marsh-Armstrong, E. B. Miller, P. Zhang, S. K. Manna, R. J. Zawadzki, N. L. Brown, T. Glaser, The *Atoh7* remote enhancer provides transcriptional robustness during retinal ganglion cell development. *Proc. Natl. Acad. Sci. U.S.A.* **117**, 21690–21700 (2020).
15. W. D. Ramdas, L. M. E. van Koolwijk, H. G. Lemij, F. Pasutto, A. J. Cree, G. Thorleifsson, S. F. Janssen, T. B. Jacoline, N. Amin, F. Rivadeneira, R. C. W. Wolfs, G. B. Walters, F. Jonasson, N. Weisschuh, C. Y. Mardin, J. Gibson, R. H. C. Zegers, A. Hofman, P. T. V. M. de Jong, A. G. Uitterlinden, B. A. Oostra, U. Thorsteinsdottir, E. Gramer, U. C. Welgen-Lüssen, J. F. Kirwan, A. A. B. Bergen, A. Reis, K. Stefansson, A. J. Lotery, J. R. Vingerling, N. M. Jansonius, C. C. W. Klaver, C. M. van Duijn, Common genetic variants associated with open-angle glaucoma. *Hum. Mol. Genet.* **20**, 2464–2471 (2011).
16. B. J. Fan, D. Y. Wang, L. R. Pasquale, J. L. Haines, J. L. Wiggs, Genetic variants associated with optic nerve vertical cup-to-disc ratio are risk factors for primary open angle glaucoma in a US caucasian population. *Invest. Opthalmol. Vis. Sci.* **52**, 1788–1792 (2011).
17. M. M. Edwards, D. S. McLeod, R. Li, R. Grebe, I. Bhutto, X. Mu, G. A. Lutty, The deletion of *Math5* disrupts retinal blood vessel and glial development in mice. *Exp. Eye Res.* **96**, 147–156 (2012).
18. M. L. O'Sullivan, V. M. Puñal, P. C. Kerstein, J. A. Brzezinski IV, T. Glaser, K. M. Wright, J. N. Kay, Astrocytes follow ganglion cell axons to establish an angiogenic template during retinal development. *Glia* **65**, 1697–1716 (2017).
19. R. W. Young, Cell differentiation in the retina of the mouse. *Anat. Rec.* **212**, 199–205 (1985).
20. R. L. Sidman, Histogenesis of mouse retina studied with Thymidine-H-3, in *Anatomica Record* (DIV JOHN WILEY & SONS INC., New York, 1960) vol. 136, pp. 276–277.
21. N. L. Brown, S. Kanekar, M. L. Vetter, P. K. Tucker, D. L. Gemza, T. Glaser, Math5 encodes a murine basic helix-loop-helix transcription factor expressed during early stages of retinal neurogenesis. *Development* **125**, 4821–4833 (1998).
22. L. Prasov, T. Glaser, Pushing the envelope of retinal ganglion cell genesis: Context dependent function of *Math5* (*Atoh7*). *Dev. Biol.* **368**, 214–230 (2012).
23. B. S. Clark, G. L. Stein-O'Brien, F. Shiau, G. H. Cannon, E. Davis-Marcisak, T. Sherman, C. P. Santiago, T. V. Hoang, F. Rajaii, R. E. James-Esposito, R. M. Gronostajski, E. J. Fertig, L. A. Goff, S. Blackshaw, Single-cell RNA-Seq analysis of retinal development identifies NFI factors as regulating mitotic exit and late-born cell specification. *Neuron* **102**, 1111–1126. e5 (2019).
24. D. H. Rapaport, L. L. Wong, E. D. Wood, D. Yasumura, M. M. LaVail, Timing and topography of cell genesis in the rat retina. *J. Comp. Neurol.* **474**, 304–324 (2004).
25. L. Feng, Z.-h. Xie, Q. Ding, X. Xie, R. T. Libby, L. Gan, MATH5 controls the acquisition of multiple retinal cell fates. *Mol. Brain* **3**, 36 (2010).

26. M. Pacal, R. Bremner, Induction of the ganglion cell differentiation program in human retinal progenitors before cell cycle exit: Kinetics of ganglion cell differentiation. *Dev. Dynam.* **243**, 712–729 (2014).
27. J. B. Miesfeld, T. Glaser, N. L. Brown, The dynamics of native Atoh7 protein expression during mouse retinal histogenesis, revealed with a new antibody. *Gene Exp. Patterns* **27**, 114–121 (2018).
28. Y. Lu, F. Shiau, W. Yi, S. Lu, Q. Wu, J. D. Pearson, A. Kallman, S. Zhong, T. Hoang, Z. Zuo, F. Zhao, M. Zhang, N. Tsai, Y. Zhuo, S. He, J. Zhang, G. L. Stein-O'Brien, T. D. Sherman, X. Duan, E. J. Fertig, L. A. Goff, D. J. Zack, J. T. Handa, T. Xue, R. Bremner, S. Blackshaw, X. Wang, B. S. Clark, Single-cell analysis of human retina identifies evolutionarily conserved and species-specific mechanisms controlling development. *Dev. Cell* **53**, 473–491.e9 (2020).
29. J. G. Aparicio, H. Hopp, A. Choi, J. M. Comar, V. C. Liao, N. Harutyunyan, T. C. Lee, Temporal expression of CD184(CXCR4) and CD171(L1CAM) identifies distinct early developmental stages of human retinal ganglion cells in embryonic stem cell derived retina. *Exp. Eye Res.* **154**, 177–189 (2017).
30. R. B. Hufnagel, A. N. Riesenberg, M. Quinn, J. A. Brzezinski, T. Glaser, N. L. Brown, Heterochronic misexpression of *Ascl1* in the *Atoh7* retinal cell lineage blocks cell cycle exit. *Mol. Cell. Neurosci.* **54**, 108–120 (2013).
31. X.-M. Zhang, T. Hashimoto, R. Tang, X.-J. Yang, Elevated expression of human bHLH factor ATOH7 accelerates cell cycle progression of progenitors and enhances production of avian retinal ganglion cells. *Sci. Rep.* **8**, 6823 (2018).
32. L. Pan, M. Deng, X. Xie, L. Gan, ISL1 and BRN3B co-regulate the differentiation of murine retinal ganglion cells. *Development* **135**, 1981–1990 (2008).
33. A. J. Pittman, M.-Y. Law, C.-B. Chien, Pathfinding in a large vertebrate axon tract: Isotypic interactions guide retinotectal axons at multiple choice points. *Development* **135**, 2865–2871 (2008).
34. L. Gan, S. W. Wang, Z. Huang, W. H. Klein, POU domain factor Brn-3b is essential for retinal ganglion cell differentiation and survival but not for initial cell fate specification. *Dev. Biol.* **210**, 469–480 (1999).
35. C.-A. Mao, J.-H. Cho, J. Wang, Z. Gao, P. Pan, W.-W. Tsai, X. Mu, L. J. Frishman, W. H. Klein, Reprogramming amacrine and photoreceptor progenitors into retinal ganglion cells by replaceing Neurod1 with Atoh7. *Development* **140**, 2849–2849 (2013).
36. C.-A. Mao, S. W. Wang, P. Pan, W. H. Klein, Rewiring the retinal ganglion cell gene regulatory network: Neurod1 promotes retinal ganglion cell fate in the absence of Math5. *Development* **135**, 3379–3388 (2008).
37. F. Wu, T. J. Kaczynski, S. Sethuramanujam, R. Li, V. Jain, M. Slaughter, X. Mu, Two transcription factors, Pou4f2 and Isl1, are sufficient to specify the retinal ganglion cell fate. *Proc. Natl. Acad. Sci. U.S.A.* **112**, E1559–E1568 (2015).
38. S.-i. Ohnuma, S. Hopper, K. C. Wang, A. Philpott, W. A. Harris, Co-ordinating retinal histogenesis: Early cell cycle exit enhances early cell fate determination in the *Xenopus* retina. *Development* **129**, 2435–2446 (2002).
39. X. Mu, X. Fu, H. Sun, P. D. Beremand, T. L. Thomas, W. H. Klein, A gene network downstream of transcription factor Math5 regulates retinal progenitor cell competence and ganglion cell fate. *Dev. Biol.* **280**, 467–481 (2005).
40. Z. Yang, K. Ding, L. Pan, M. Deng, L. Gan, Math5 determines the competence state of retinal ganglion cell progenitors. *Dev. Biol.* **264**, 240–254 (2003).
41. L. Poggi, M. Vitorino, I. Masai, W. A. Harris, Influences on neural lineage and mode of division in the zebrafish retina in vivo. *J. Cell Biol.* **171**, 991–999 (2005).
42. S.-K. Chen, K. S. Chew, D. S. McNeill, P. W. Keeley, J. L. Ecker, B. Q. Mao, J. Pahlberg, B. Kim, S. C. S. Lee, M. A. Fox, W. Guido, K. Y. Wong, A. P. Sampath, B. E. Reese, R. Kuruvilla, S. Hattar, Apoptosis regulates ipRGC spacing necessary for rods and cones to drive circadian photoentrainment. *Neuron* **77**, 503–515 (2013).
43. C. M. Knudson, K. S. K. Tung, W. G. Tourtellotte, G. A. J. Brown, S. J. Korsmeyer, Bax-deficient mice with lymphoid hyperplasia and male germ cell death. *Science* **270**, 96–99 (1995).
44. X. Mu, X. Fu, P. D. Beremand, T. L. Thomas, W. H. Klein, Gene-regulation logic in retinal ganglion cell development: Isl1 defines a critical branch distinct from but overlapping with Pou4f2. *Proc. Natl. Acad. Sci. U.S.A.* **105**, 6942–6947 (2008).
45. R. W. Young, Cell death during differentiation of the retina in the mouse. *J. Comp. Neurol.* **229**, 362–373 (1984).
46. M. O. Péquignot, A. C. Provost, S. Sallé, P. Taupin, K. M. Sainton, D. Marchant, J. C. Martinou, J. C. Ameisen, J.-P. Jais, M. Abitbol, Major role of BAX in apoptosis during retinal development and in establishment of a functional postnatal retina. *Dev. Dynam.* **228**, 231–238 (2003).
47. J. M. Ogilvie, T. L. Deckwerth, C. M. Knudson, S. J. Korsmeyer, Suppression of developmental retinal cell death but not of photoreceptor degeneration in Bax-deficient mice. *Invest. Ophthalmol. Visual Sci.* **39**, 1713–1720 (1998).
48. A. R. Rodriguez, L. Pérez de Sevilla Müller, N. C. Brecha, The RNA binding protein RBPMS is a selective marker of ganglion cells in the mammalian retina. *J. Comp. Neurol.* **522**, 1411–1443 (2014).
49. M. Xiang, L. Zhou, J. P. Macke, T. Yoshioka, S. H. Hendry, R. L. Eddy, T. B. Shows, J. Nathans, The Brn-3 family of POU-domain factors: Primary structure, binding specificity, and expression in subsets of retinal ganglion cells and somatosensory neurons. *J. Neurosci.* **15**, 4762–4785 (1995).
50. X. Mu, P. D. Beremand, S. Zhao, R. Pershad, H. Sun, A. Scarpa, S. Liang, T. L. Thomas, W. H. Klein, Discrete gene sets depend on POU domain transcription factor Brn3b/Brn-3.2/POU4f2 for their expression in the mouse embryonic retina. *Development* **131**, 1197–1210 (2004).
51. S.-K. Chen, T. C. Badea, S. Hattar, Photoentrainment and pupillary light reflex are mediated by distinct populations of ipRGCs. *Nature* **476**, 92–95 (2011).
52. S. Rowan, C. L. Cepko, Genetic analysis of the homeodomain transcription factor Chx10 in the retina using a novel multifunctional BAC transgenic mouse reporter. *Dev. Biol.* **271**, 388–402 (2004).
53. Y. V. Wang, M. Weick, J. B. Demb, Spectral and temporal sensitivity of cone-mediated responses in mouse retinal ganglion cells. *J. Neurosci.* **31**, 7670–7681 (2011).
54. D. M. Berson, F. A. Dunn, M. Takao, Phototransduction by retinal ganglion cells that set the circadian clock. *Science* **295**, 1070–1073 (2002).
55. S. Hattar, H.-W. Liao, M. Takao, D. M. Berson, K.-W. Yau, Melanopsin-containing retinal ganglion cells: Architecture, projections, and intrinsic photosensitivity. *Science* **295**, 1065–1070 (2002).
56. M. T. H. Do, K.-W. Yau, Intrinsically photosensitive retinal ganglion cells. *Physiol. Rev.* **90**, 1547–1581 (2010).
57. M. T. H. Do, Melanopsin and the intrinsically photosensitive retinal ganglion cells: Biophysics to behavior. *Neuron* **104**, 205–226 (2019).
58. Q. Shi, P. Gupta, A. K. Boukhvalova, J. H. Singer, D. A. Butts, Functional characterization of retinal ganglion cells using tailored nonlinear modeling. *Sci. Rep.* **9**, 8713 (2019).
59. J. W. Triplett, C. Pfeiffenberger, J. Yamada, B. K. Stafford, N. T. Sweeney, A. M. Litke, A. Sher, A. A. Koulakov, D. A. Feldheim, Competition is a driving force in topographic mapping. *Proc. Natl. Acad. Sci. U.S.A.* **108**, 19060–19065 (2011).
60. J. L. Bedont, T. A. Le Gates, E. A. Slat, M. S. Byerly, H. Wang, J. Hu, A. C. Rupp, J. Qian, G. W. Wong, E. D. Herzog, S. Hattar, S. Blackshaw, Lhx1 controls terminal differentiation and circadian function of the suprachiasmatic nucleus. *Cell Rep.* **7**, 609–622 (2014).
61. H. Kondo, I. Matsushita, T. Tahira, E. Uchio, S. Kusaka, Mutations in *ATOH7* gene in patients with nonsyndromic congenital retinal nonattachment and familial exudative vitreoretinopathy. *Ophthalmic Genet.* **37**, 462–464 (2016).
62. Q. L. Giudice, M. Leleu, G. L. Manno, P. J. Fabre, Single-cell transcriptional logic of cell-fate specification and axon guidance in early born retinal neurons. *Development* **146**, dev178103 (2019).
63. R. B. Hufnagel, T. T. Le, A. L. Riesenberg, N. L. Brown, Neurog2 controls the leading edge of neurogenesis in the mammalian retina. *Dev. Biol.* **340**, 490–503 (2010).
64. H. Zhou, T. Yoshioka, J. Nathans, Retina-derived POU-domain factor-1: A complex POU-domain gene implicated in the development of retinal ganglion and amacrine cells. *J. Neurosci.* **16**, 2261–2274 (1996).
65. S. W. Choy, C. W. Cheng, S. T. Lee, V. W. T. Li, M. N. Y. Hui, C.-C. Hui, D. Liu, S. H. Cheng, A cascade of irx1a and irx2a controls shh expression during retinogenesis. *Dev. Dyn.* **239**, 3204–3214 (2010).
66. P. Ekström, K. Johansson, Differentiation of ganglion cells and amacrine cells in the rat retina: Correlation with expression of HuC/D and GAP-43 proteins. *Dev. Brain Res.* **145**, 1–8 (2003).
67. K. Kruger, A. S. Tam, C. Lu, D. W. Sretavan, Retinal ganglion cell axon progression from the optic chiasm to initiate optic tract development requires cell autonomous function of GAP-43. *J. Neurosci.* **18**, 5692–5705 (1998).
68. P. Panza, A. A. Sitko, H.-M. Maischein, I. Koch, M. Flötenmeyer, G. J. Wright, K. Mandai, C. A. Mason, C. Söllner, The LRR receptor Islr2 is required for retinal axon routing at the vertebrate optic chiasm. *Neural Dev.* **10**, 23 (2015).
69. J. B. Miesfeld, M.-s. Moon, A. N. Riesenberg, A. N. Contreras, R. A. Kovall, N. L. Brown, Rbpj direct regulation of *Atoh7* transcription in the embryonic mouse retina. *Sci. Rep.* **8**, 10195 (2018).
70. K. B. Moore, M. A. Logan, I. Aldiri, J. M. Roberts, M. Steele, M. L. Vetter, C8orf46 homolog encodes a novel protein Vexin that is required for neurogenesis in *Xenopus laevis*. *Dev. Biol.* **437**, 27–40 (2018).
71. P. Bhansali, I. Rayport, A. Rebsam, C. Mason, Delayed neurogenesis leads to altered specification of ventrotemporal retinal ganglion cells in albino mice. *Neural Dev.* **9**, 11 (2014).
72. F. A. Wolf, P. Angerer, F. J. Theis, SCANPY: Large-scale single-cell gene expression data analysis. *Genome Biol.* **19**, 15 (2018).
73. F. Wu, J. E. Bard, J. Kann, D. Yergeau, D. Sapkota, Y. Ge, Z. Hu, J. Wang, T. Liu, X. Mu, Single cell transcriptomics reveals lineage trajectory of the retinal ganglion cells in wild-type and *Atoh7*-null retinas. *Biorxiv* 2020.02.26.966093, (2020).
74. G. L. Stein-O'Brien, B. S. Clark, T. Sherman, C. Zibetti, Q. Hu, R. Sealfon, S. Liu, J. Qian, C. Colantuoni, S. Blackshaw, L. A. Goff, E. J. Fertig, Decomposing cell identity for transfer

learning across cellular measurements, platforms, tissues, and species. *Cell Syst.* **8**, 395–411.e8 (2019).
75. C. Guo, K.-S. Cho, Y. Li, K. Tchedre, C. Antolik, J. Ma, J. Chew, T. P. Utheim, X. A. Huang, H. Yu, M. T. A. Malik, N. Anzak, D. F. Chen, IGFBPL1 regulates axon growth through IGF-1-mediated signaling cascades. *Sci. Rep.* **8**, 2054 (2018).
76. F. Zhang, C. Lu, C. Severin, D. W. Sretavan, GAP-43 mediates retinal axon interaction with lateral diencephalon cells during optic tract formation. *Development* **127**, 969–980 (2000).
77. I. Soto, E. Oglesby, B. P. Buckingham, J. L. Son, E. D. O. Roberson, M. R. Steele, D. M. Inman, M. L. Vetter, P. J. Horner, N. Marsh-Armstrong, Retinal ganglion cells downregulate gene expression and lose their axons within the optic nerve head in a mouse glaucoma model. *J. Neurosci.* **28**, 548–561 (2008).
78. N. M. Tran, K. Shekhar, I. E. Whitney, A. Jacobi, I. Benhar, G. Hong, W. Yan, X. Adiconis, M. E. Arnold, J. M. Lee, J. Z. Levin, D. Lin, C. Wang, C. M. Lieber, A. Regev, Z. He, J. R. Sanes, Single-cell profiles of retinal ganglion cells differing in resilience to injury reveal neuroprotective genes. *Neuron* **104**, 1039–1055.e12 (2019).
79. B. A. Rheaume, A. Jereen, M. Bolisetty, M. S. Sajid, Y. Yang, K. Renna, L. Sun, P. Robson, E. F. Trakhtenberg, Single cell transcriptome profiling of retinal ganglion cells identifies cellular subtypes. *Nat. Commun.* **9**, 2759 (2018).
80. P. J. Skene, S. Henikoff, An efficient targeted nuclease strategy for high-resolution mapping of DNA binding sites. *eLife* **6**, e21856 (2017).
81. Y. Zhang, T. Liu, C. A. Meyer, J. Eeckhoute, D. S. Johnson, B. E. Bernstein, C. Nusbaum, R. M. Myers, M. Brown, W. Li, X. S. Liu, Model-based analysis of ChIP-Seq (MACS). *Genome Biol.* **9**, R137 (2008).
82. I. Aldiri, B. Xu, L. Wang, X. Chen, D. Hiler, L. Griffiths, M. Valentine, A. Shirinifard, S. Thiagarajan, A. Sablauer, M.-E. Barabas, J. Zhang, D. Johnson, S. Frase, X. Zhou, J. Easton, J. Zhang, E. R. Mardis, R. K. Wilson, J. R. Downing, M. A. Dyer; St. Jude Children's Research Hospital – Washington University Pediatric Cancer Genome Project, The dynamic epigenetic landscape of the retina during development, reprogramming, and tumorigenesis. *Neuron* **94**, 550–568.e10 (2017).
83. S. Heinz, C. Benner, N. Spann, E. Bertolino, Y. C. Lin, P. Laslo, J. X. Cheng, C. Murre, H. Singh, C. K. Glass, Simple combinations of lineage-determining transcription factors prime cis-regulatory elements required for macrophage and B cell identities. *Mol. Cell* **38**, 576–589 (2010).
84. G. Yu, L.-G. Wang, Q.-Y. He, ChIPseeker: An R/Bioconductor package for ChIP peak annotation, comparison and visualization. *Bioinformatics* **31**, 2382–2383 (2015).
85. O. Cordero-Llana, F. Rinaldi, P. A. Brennan, D. Wynick, M. A. Caldwell, Galanin promotes neuronal differentiation from neural progenitor cells in vitro and contributes to the generation of new olfactory neurons in the adult mouse brain. *Exp. Neurol.* **256**, 93–104 (2014).
86. F. E. Holmes, S. Mahoney, V. R. King, A. Bacon, N. C. H. Kerr, V. Pachnis, R. Curtis, J. V. Priestley, D. Wynick, Targeted disruption of the galanin gene reduces the number of sensory neurons and their regenerative capacity. *Proc. Natl. Acad. Sci. U.S.A.* **97**, 11563–11568 (2000).
87. N. E. Baker, N. L. Brown, All in the family: Proneural bHLH genes and neuronal diversity. *Development* **145**, dev159426 (2018).
88. A. I. Valenciano, P. Boya, E. J. de la Rosa, Early neural cell death: Numbers and cues from the developing neuroretina. *Int. J. Dev. Biol.* **53**, 1515–1528 (2009).
89. J. M. Frade, P. Bovolenta, J. R. Martínez-Morales, A. Arribas, J. A. Barbas, A. Rodríguez-Tébar, Control of early cell death by BDNF in the chick retina. *Development* **124**, 3313–3320 (1997).
90. L. Rodríguez-Gallardo, M. del Carmen Lineros-Domínguez, J. Francisco-Morcillo, G. Martín-Partido, Macrophages during retina and optic nerve development in the mouse embryo: Relationship to cell death and optic fibres. *Anat. Embryol.* **210**, 303–316 (2005).
91. R. C. Strom, R. W. Williams, Cell production and cell death in the generation of variation in neuron number. *J. Neurosci.* **18**, 9948–9953 (1998).
92. M. H. Farah, S. S. Easter Jr., Cell birth and death in the mouse retinal ganglion cell layer. *J. Comp. Neurol.* **489**, 120–134 (2005).
93. T. T. Le, E. Wroblewski, S. Patel, A. N. Riesenberg, N. L. Brown, *Math5* is required for both early retinal neuron differentiation and cell cycle progression. *Dev. Biol.* **295**, 764–778 (2006).
94. J. Yao, X. Sun, Y. Wang, L. Wang, Muller glia induce retinal progenitor cells to differentiate into retinal ganglion cells. *Neuroreport* **17**, 1263–1267 (2006).
95. M. Chen, Q. Chen, X. Sun, W. Shen, B. Liu, X. Zhong, Y. Leng, C. Li, W. Zhang, F. Chai, B. Huang, Q. Gao, A. P. Xiang, Y. Zhuo, J. Ge, Generation of retinal ganglion-like cells from reprogrammed mouse fibroblasts. *Invest. Ophthalmol. Vis. Sci.* **51**, 5970–5978 (2010).
96. W.-t. Song, Q. Zeng, X.-b. Xia, K. Xia, Q. Pan, Atoh7 promotes retinal Müller cell differentiation into retinal ganglion cells. *Cytotechnology* **68**, 267–277 (2016).
97. W.-t. Song, X.-y. Zhang, X.-b. Xia, Atoh7 promotes the differentiation of Müller cells-derived retinal stem cells into retinal ganglion cells in a rat model of glaucoma. *Exp. Biol. Med.* **240**, 682–690 (2015).
98. Y. Jiang, Q. Ding, X. Xie, R. T. Libby, V. Lefebvre, L. Gan, Transcription factors SOX4 and SOX11 function redundantly to regulate the development of mouse retinal ganglion cells. *J. Biol. Chem.* **288**, 18429–18438 (2013).
99. D. Sapkota, H. Chintala, F. Wu, S. J. Fliesler, Z. Hu, X. Mu, Onecut1 and Onecut2 redundantly regulate early retinal cell fates during development. *Proc. Natl. Acad. Sci. U.S.A.* **111**, E4086–E4095 (2014).
100. O. Takeuchi, J. Fisher, H. Suh, H. Harada, B. A. Malynn, S. J. Korsmeyer, Essential role of BAX, BAK in B cell homeostasis and prevention of autoimmune disease. *Proc. Natl. Acad. Sci. U.S.A.* **102**, 11272–11277 (2005).
101. L. Madisen, T. A. Zwingman, S. M. Sunkin, S. W. Oh, H. A. Zariwala, H. Gu, L. L. Ng, R. D. Palmiter, M. J. Hawrylycz, A. R. Jones, E. S. Lein, H. Zeng, A robust and high-throughput Cre reporting and characterization system for the whole mouse brain. *Nat. Neurosci.* **13**, 133–140 (2010).
102. T. C. Badea, H. Cahill, J. Ecker, S. Hattar, J. Nathans, Distinct roles of transcription factors Brn3a and Brn3b in controlling the development, morphology, and function of retinal ganglion cells. *Neuron* **61**, 852–864 (2009).
103. J. M. McFarland, Y. Cui, D. A. Butts, Inferring nonlinear neuronal computation based on physiologically plausible inputs. *PLOS Comput. Biol.* **9**, e1003143 (2013).
104. T. D. Sherman, T. Gao, E. J. Fertig, CoGAPS 3: Bayesian non-negative matrix factorization for single-cell analysis with asynchronous updates and sparse data structures. *bioRxiv*, 699041 (2019).
105. L. Haghverdi, M. Büttner, F. A. Wolf, F. Buettner, F. J. Theis, Diffusion pseudotime robustly reconstructs lineage branching. *Nat. Methods* **13**, 845–848 (2016).
106. K. Polański, M. D. Young, Z. Miao, K. B. Meyer, S. A. Teichmann, J.-E. Park, BBKNN: Fast batch alignment of single cell transcriptomes. *Bioinformatics* **36**, 964–965 (2019).
107. C. Trapnell, D. Cacchiarelli, J. Grimsby, P. Pokharel, S. Li, M. Morse, N. J. Lennon, K. J. Livak, T. S. Mikkelsen, J. L. Rinn, The dynamics and regulators of cell fate decisions are revealed by pseudotemporal ordering of single cells. *Nat. Biotechnol.* **32**, 381–386 (2014).
108. X. Qiu, A. Hill, J. Packer, D. Lin, Y.-A. Ma, C. Trapnell, Single-cell mRNA quantification and differential analysis with Census. *Nat. Methods* **14**, 309–315 (2017).
109. T. Shimogori, D. A. Lee, A. Miranda-Angulo, Y. Yang, H. Wang, L. Jiang, A. C. Yoshida, A. Kataoka, H. Mashiko, M. Avetisyan, L. Qi, J. Qian, S. Blackshaw, A genomic atlas of mouse hypothalamic development. *Nat. Neurosci.* **13**, 767–775 (2010).
110. B. Langmead, S. L. Salzberg, Fast gapped-read alignment with Bowtie 2. *Nat. Methods* **9**, 357–359 (2012).
111. M. P. Meers, T. D. Bryson, J. G. Henikoff, S. Henikoff, Improved CUT&RUN chromatin profiling tools. *eLife* **8**, e46314 (2019).
112. H. Li, B. Handsaker, A. Wysoker, T. Fennell, J. Ruan, N. Homer, G. Marth, G. Abecasis, R. Durbin; 1000 Genome Project Data Processing Subgroup, The Sequence Alignment/Map format and SAMtools. *Bioinformatics* **25**, 2078–2079 (2009).
113. A. R. Quinlan, I. M. Hall, BEDTools: A flexible suite of utilities for comparing genomic features. *Bioinformatics* **26**, 841–842 (2010).
114. F. Ramírez, D. P. Ryan, B. Grüning, V. Bhardwaj, F. Kilpert, A. S. Richter, S. Heyne, F. Dündar, T. Manke, deepTools2: A next generation web server for deep-sequencing data analysis. *Nucleic Acids Res.* **44**, W160–W165 (2016).
115. R. Morris, Developments of a water-maze procedure for studying spatial learning in the rat. *J Neurosci Meth.* **11**, 47–60 (1984).
116. P. Mombaerts, F. Wang, C. Dulac, S. K. Chao, A. Nemes, M. Mendelsohn, J. Edmondson, R. Axel, Visualizing an olfactory sensory map. *Cell* **87**, 675–686 (1996).

Acknowledgments: We thank X. Mu and F. Wu for providing *Atoh7*$^{tTA/tTA}$*;B&I-EE* mice, L. Gan for providing *Atoh7*^{Cre} mice, N. Brown for technical advice, H. Hao and Hopkins Transcriptomics and Deep-Sequencing Core for assistance with scRNA-seq, and W. Yap for comments on the manuscript. **Funding:** This work was supported by NIH grants R01EY020560 (S.B.), R00EY27844 (B.S.C.), EY19497 (T.G.), GM076430 and EY027202 (S.H. and H.Z.), EY021372 (J.S.), and F32 EY022543 (T.S.); the intramural research fund at the National Institute of Mental Health (MH002964) (S.H.); an unrestricted grant to the Department of Ophthalmology and Visual Sciences from Research to Prevent Blindness (B.S.C. and P.A.R.); and grants from the Krembil Foundation/Brain Canada and the Canadian Institutes of Health Research FDN-159936 (M.C.). **Author contributions:** J.B.-K., B.S.C., S.B., S.H., and T.S. conceived and planned the study. B.S.C., F.S., D.W.K., and J.B.-K. performed the scRNA-seq, analyzed by B.S.C., F.S., and A.J. M.F. and M.C. performed the Cut&Run experiment, analyzed by B.S.C., F.S., P.A.R., and J.S. Q.S. performed and analyzed the MEA analysis. J.L. performed and analyzed the PLR experiments. T.B. and T.G. provided reagents and guidance. C.S. performed non-PLR behavior experiments. J.B.-K. performed all other experiments. J.B.-K., B.S.C., S.B., M.C., and S.H. prepared the manuscript with guidance from all authors. S.H., B.S.C., S.B., M.C., J.S., and H.Z. provided funding. **Competing interests:** The authors declare that they have no competing interests.

Data and materials availability: All data needed to evaluate the conclusions in the paper are present in the paper and/or the Supplementary Materials. scRNA-seq–processed [expression, gene (featureData), and cell (phenoData) matrices] and raw sequence information (.bam files) are available for direct download through GEO GSE148814. Atoh7 Cut&Run data are available through GEO GSE156756. The mouse developmental scRNA-seq (*23*) and ATAC-seq datasets were downloaded from GSE118614 and GSE102092, respectively. ATAC-seq samples were realigned to mm10, to conform to scRNA-seq and Cut&Run datasets using the same pipeline as described for Cut&Run samples. Additional data related to this paper may be requested from the authors.

Submitted 25 August 2020
Accepted 29 January 2021
Published 12 March 2021
10.1126/sciadv.abe4983

Citation: J. Brodie-Kommit, B. S. Clark, Q. Shi, F. Shiau, D. W. Kim, J. Langel, C. Sheely, P. A. Ruzycki, M. Fries, A. Javed, M. Cayouette, T. Schmidt, T. Badea, T. Glaser, H. Zhao, J. Singer, S. Blackshaw, S. Hattar, Atoh7-independent specification of retinal ganglion cell identity. *Sci. Adv.* **7**, eabe4983 (2021).